Laser Frequency Stabilization for Trapped Yb^+ Experiments

by

Deon Anton Janse van Rensburg

Thesis presented in partial fulfilment of the requirements for the degree of Master of Science (Physics) in the Faculty of Science at Stellenbosch University

Supervisor: Dr. C. Steenkamp

December 2020

The financial assistance of the National Research Foundation (NRF) towards this research is hereby acknowledged. Opinions expressed and conclusions arrived at, are those of the author and are not necessarily to be attributed to the NRF.

Declaration

By submitting this thesis electronically, I declare that the entirety of the work contained therein is my own, original work, that I am the sole author thereof (save to the extent explicitly otherwise stated), that reproduction and publication thereof by Stellenbosch University will not infringe any third party rights and that I have not previously in its entirety or in part submitted it for obtaining any qualification.

Date: December 2020 .....

Abstract

Laser Frequency Stabilization for Trapped Yb^+ Experiments

D.A. Janse van Rensburg

Department of Physics,
Stellenbosch University,
Private Bag X1, 7602 Matieland, South Africa.

Thesis: MSc (Physics)

December 2020

This project sets out to frequency stabilize external cavity diode lasers of wavelengths $\lambda = 935$ nm and 739 nm, with an eye to Ytterbium-171 ion trapping. The desired laser linewidths were below 1 MHz at 1 second observation time and the desired long term frequency drifts were below a megahertz over the course of a few hours. To stabilize the lasers, two Pound-Drever-Hall laser frequency stabilisation systems were designed, constructed and characterized. The optical frequency references used were sub-megahertz linewidth optical cavities with Invar spacers. These cavities were designed and constructed in-house. The achieved long term stability of the stabilized lasers was 1 MHz/h over a 5 hour measurement period. The laser frequency long term stabilities are limited by the thermal stabilities of the cavity spacers. The post stabilisation laser frequency noise was lowered when compared to the free running lasers. This was observed by determining the laser frequency noise power spectral densities. From the frequency noise power spectral densities lower bounds on the locked laser linewidths were established. This lower bound is 11.92 kHz for the 739 nm wavelength laser at 1 second observation time and 5.4 kHz for the 935 nm wavelength laser. An additional system was designed and constructed

to stabilize the 935 nm wavelength laser to an in-house built piezo electrically tunable cavity noise power spectral densities to simultaneously stabilize the length of the cavity to a microwave frequency referenced to a Rubidium frequency standard. Technical limitations (optical feedback into the the 935 nm wavelength laser cavity) prohibited the implementation of a stable lock of the cavity length.

Uittreksel

Laserfrekwensie Stabiliseering vir Vasgevange Yb^+ Eksperimente

("Laser Frequency Stabilization for Trapped Yb^+ Experiments")

D.A. Janse van Rensburg

Departement Fisika,
Universiteit Stellenbosch,
Privaatsak X1, 7602 Matieland, Suid Afrika.

Tesis: MSc (Fisika)

Desember 2020

Die doel van die projek is om die frekwensies van diodelasers met eksterne resonansholtes te stabiliseer. Die lasers, met golflengtes $\lambda = 935$ nm en 739 nm, vorm deel van 'n Ytterbium 171 ioonval Die mikpunt was om die laserlynwydte te vernou tot minder as 1 MHz vir 'n sekond lange meeting. Die langtermyn dryf van die laser frekwensies moes ook tot minder as 'n MHz oor 'n paar uur verminder word. Om die lasers te stabiliseer is twee Pound-Drever-Hall laserfrekwensie stabiliseerings sisteme ontwerp, gebou en getoets. Die optiese frekwensie verwysings is twee optiese holtes wat ook ontwerp en gebou is vir hierdie projek. Die langtermyn dryf van die gestibilseerde lasers was 1 MHz/h, soos beperk deur die termiese stabiliteit van die optiese holtes se lengtes. 'n Vermindering in die gestabaliseerde laserslynwydte is waargeneem. Hierdie is bepaal deur die frewkwensie geraas van die lasers te meet. Die gemete laser frekwensie geraas is gebruik om die minimum verwagte laser lynwydtes vas te stel. Hierdie waardes is bepaal as 11.92 kHz vir die 739 nm golflengte laser vir 'n sekonde lange meeting en 5.4 kHz vir die 935 nm golflengte laser. 'n Addisionele optiese holte met verstelbare lengte is ook ontwerp en gebou.

Hierdie holte het deel gevorm van ’n sisteem wat die laser met die hulp van ’n optiese holte stabiliseer en tergelyktydig die lengte van die holte met behulp van ’n stabiele mikrogolf frekwensie stabilisieer. Hierdie sisteem is onsuksesvol weens tegniese probleme, naamlik optiese terugvoer in die laser in.

Acknowledgements

I would like to thank Prof M. Thame for his assistance in providing the funding from the NRF, Dr C. Steenkamp for serving as supervisor for this project and Ms. Nancy Payne for her support in the lab.

I extend my greatest gratitude to Prof H. Uys for his support and mentorship as well as for providing the funding as the CSIR/SU joint Chair in Atomic, Molecular and Optical Physics.

To my fellow students, the academic staff, support staff and technical staff of the physics department, thank you for making the long hours spent in the Merensky building enjoyable.

Lastly, to my friends and family, I could not have done this without you.

Dankie.

Contents

List of Figures

List of Tables

Chapter 1

Introduction

Wolfgang Paul and Hans Georg Dehmelt developed the ion trap technique for which they shared one-half of the 1989 Nobel Prize in Physics. Trapped ions are spatially confined by electric and/or magnetic fields in ultra-high vacuum to isolate them from other particles which might perturb the state of the ion, allowing for long interrogation times of the unperturbed ion [1]. The long interrogation times are of great advantage for metrology purposes with trapped ions used for high precision measurements, for example Brewer *et al.* [2] used the $^1S_0 \leftrightarrow {}^3P_0$ transition of trapped $^{27}Al^+$ to produce an optical clock with fractional frequency uncertainty of $\delta\nu/\nu = 9.4 \times 10^{-19}$. This is the lowest systematic uncertainty of any clock as of the date of writing. The trapped ion quantum computer is also a proposed architecture for a large scale quantum computer [3] with CNOT quantum gates constructed from trapped $^9Be^+$ ions by Monroe *et al.* [4] in 1995. This proposed architecture will use the ground state hyperfine levels of the ion as the quantum bit, forming what is referred to as a hyperfine qubit [5].

The Trapped Ion Quantum Control research group at Stellenbosch University's Department of Physics is interested in using trapped $^{171}Yb^+$ hyperfine qubits for metrology and quantum measurement theory experiments. Qubits are quantum systems which can be interacted with by using electromagnetic radiation. The scale at which quantum mechanical phenomena can be observed necessitates the use of sensitive laboratory instrumentation. Due to the narrow transition linewidth of these qubits, frequency stable and spectrally narrow lasers are required for control of the qubits and for making precision measurements. This project is focused on reducing the linewidth and the

frequency drift of two external cavity diode lasers which are used in the ion trapping laboratory.

Frequency stabilized lasers are not only necessary tools in ion trapping laboratories, they have been used for experiments in fields ranging from general relativity to quantum electrodynamics. Frequency stabilized lasers are used as measurement tools to measure accurate displacements, time delays and frequencies, this has made them useful in a wide range of applications such as in the observation of gravitational waves [6], geophysical strain observations [7] and spectroscopy of antihydrogen [8].

The goal of this project was to reduce the linewidths of the 739 nm wavelength and 935 nm wavelength lasers to below a megahertz at 1 second observation time and to reduce their long term frequency drift to below a megahertz over a few hours. To achieve this goal, three optical reference cavities were designed and built, a fixed length cavity for each of the two lasers and a cavity with tunable length via a piezoelectric actuator for the 935 nm wavelength laser.

The required background knowledge such as the Yb^+ linear Paul trap, laser frequency stabilization techniques and the design considerations for the reference cavities are introduced in Chapter 2. Chapter 3 describes the design, implementation and methods for characterization of the stabilization system. Chapter 4 presents the results of these experiments and these results are used to evaluate the stabilization system performance. Chapter 5 contains the concluding remarks.

Chapter 2

Background

2.1 Yb^+ Linear Paul Trap

This section will give a brief outline on the Yb^+ linear Paul trap. This will provide some context to what the work done for this project will ultimately form part of.

The isotopes of Ytterbium of interest for the ion trapping laboratory are ^{171}Yb and ^{174}Yb which constitutes 14.216% [9] and 31.896% [9] of natural Ytterbium respectively. A selective two-photon photoionization scheme is used to trap only a single isotope of Ytterbium at a time. This scheme relies on the isotope shift of the $^1S_0 \leftrightarrow ^1P_1$ transition which has transition frequency 751 527 368.68(39) MHz [10] for ^{171}Yb (F = 3/2) and 751 526 533.49(33) MHz [10] for ^{174}Yb . With the use of narrow band, continuous wave lasers these isotope specific transition can be selectively driven to prepare only a certain isotope in a state which can then be excited to continuum by a 369 nm wavelength laser to form Yb^+. These ions can then be confined to a region of space by a linear Paul trap. This trap uses oscillating and static electric fields to create a time varying spatial electric field gradient which causes the electrically charged ion to experience a force towards the trap minimum. The ions are Doppler cooled using a 369 nm wavelength laser which is red detuned from the $^2S_{1/2} \leftrightarrow ^2P_{1/2}$ transition.

Furthermore a 935 nm wavelength laser is used to create a cycling transition which prevents the ion from transitioning to a dark state. A 638 nm wavelength laser is used to depopulate the $^2F_{7/2}$ level, to which the ion transitions infrequently. This can be observed in figure 2.1 which gives the relevant

level structure of $^{171}Yb^{+}$.

The lifetime of the $D^3[3/2]_{1/2}$ level is 37.7 ns [11] and 8.07 ns [12] for the $^2P_{1/2}$ level. This equates to natural linewidths of 4.22 MHz and 19.6 MHz respectively.

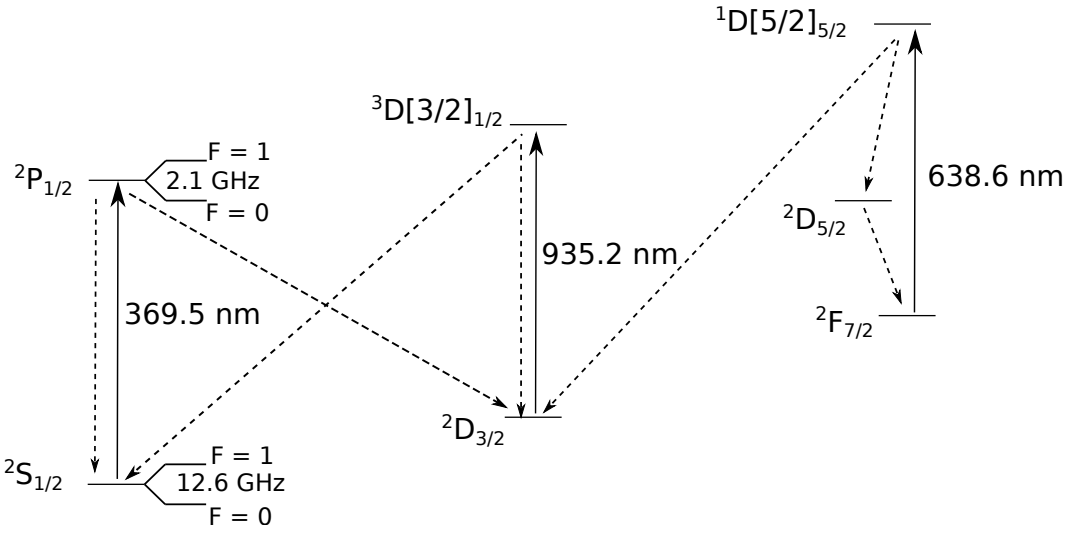

Figure 2.1: Relevant level structure of $^{171}Yb^{+}$. Laser driven transitions are shown by solid lines and allowed decay paths are shown by dashed lines. Transition energies not drawn to scale.

The $^2S_{1/2}\,|F = 0, m_F = 0\rangle$ and $^2S_{1/2}\,|F = 1, m_F = 0\rangle$ levels of $^{171}Yb^{+}$ form the hyperfine qubit states $|0\rangle$ and $|1\rangle$ respectively.

2.2 Laser Frequency Noise

The frequency noise of a laser arises from fluctuations in the phase of the laser output, since the instantaneous frequency is proportional to the time derivative of the phase. For single frequency diode lasers the dominant phase noise comprises of white noise arising from phase and refractive index fluctuations due to spontaneous emissions from the laser gain medium and flicker[1] noise from other sources [13]. A measure of the spectral purity of a laser is its spectral linewidth, which is the width of its optical power spectral density. For single frequency diode lasers the power spectral density comprises of a Lorentzian spectrum from the white noise and a Gaussian spectrum from the flicker noise

[1]Flicker noise is a classification of noise whose power spectral density has a 1/f profile.

[13]. The Lorentzian linewidth, also known as the fundamental linewidth, can be narrowed by use of an external laser cavity [14]. The flicker noise is mainly comprised of noise sources such as driver current noise and thermal expansion of the resonator. These technical noise sources can be reduced by improved design of the laser system and by means of high bandwidth frequency stabilization [13].

The laser linewdith is not a full characterization of the frequency noise of a laser. The frequency noise power spectrum of the laser provides a more descriptive measure of the frequency noise. The frequency noise spectrum can be determined with an optical frequency discriminator, such as an optical cavity or a path imbalanced Mach-Zehnder interferometer [15]. The linewidth can be determined from the frequency noise power spectral density with the reverse not possible [16]. The laser linewidth $\delta\nu$ can be estimated from an arbitrary laser frequency noise power spectral density $s(f)$ using the equation

$$\delta\nu = \left(8\ln(2)\int_{1/T_0}^{\infty} \mathrm{d}f \left(\mathrm{H}\left(s(f) - \frac{8\ln(2)f}{\pi^2}\right)s(f)\right)\right)^{1/2}, \tag{2.2.1}$$

where T_0 is the observation time of the spectral density measurement and H is the Heaviside step function. Equation 2.2.1 was derived by Di Domenico *et al.* [16] and then experimentally verified by Bucalovic *et al.* [17].

If only the laser linewidth is desired, the following methods can be used to determine it without first measuring the frequency noise power spectral density. The linewidth of a laser can be determined from the spectrum of the beat frequency of the laser under test and a stable, narrow linewidth reference laser. The beat frequency is measured on a photodetector with suitable bandwidth and the signal is analyzed with an electrical spectrum analyzer. The test laser linewidth can be deduced from the measured spectrum given knowledge of the reference laser linewidth [18].

In the absence of a stable reference laser a time delayed and frequency shifted version of the laser under test can be used as the reference beam, provided that the time delay is much longer than the coherence time of the laser, so as to remove the correlation between the reference and test beam's phases. This method is known as the Delayed Self-Hetrodyne method. The time delay can be instituted by means of an optical path delay via an optical fiber, with the fiber length required increasing with decreasing laser linewidth [19].

To reduce the length of fiber required for narrow linewidth measurements and to remove any extra phase noise acquired due to the long fiber, a modified delayed self-heterodyne measurement can be used with short delay time [20]. In the delay time shorter than coherence time regime the measured spectrum is dependent on the delay time due to filtering of low frequency noise [21]. The low frequency noise contributes to the measurement time dependence of the acquired spectrum for both short and long delays [22]. With appropriate choice of the delay time, the low frequency noise can filtered out and the fundamental linewidth can be extracted from the spectrum [23].

2.3 Laser Frequency Stabilization

For an external cavity diode laser (ECDL) there are three parameters which can be used to control the operating wavelength, namely the grating position, laser current and diode temperature with the bandwidth of the feedback highest for the current and lowest for the temperature. To improve on the frequency stability of the laser, closed loop operation can be used [24].

The operating process of a closed feedback loop is that a process output is measured, this measured value is compared to a reference value. The difference between the measured and reference value is used to generate an error value. A controller is used to determine the appropriate response to apply to the system to change the process output such that the error value will be minimized [25].

For laser frequency stabilization a suitable frequency reference is required such that the laser frequency can be compared to it. Visible light's electric field oscillates at a frequency of between 440 and 770 terahertz, making a direct measurement of optical frequencies using electronic means non-feasible. Optical frequency measurement techniques rely on the interaction of the laser light and some frequency reference to produce a lower frequency signal or a frequency dependent intensity which is used to deduce the relative frequency difference between the laser and the reference. The following section briefly describes a few optical frequency references used for laser frequency stabilization.

2.3.1 Optical Frequency References

The International System of Units (SI) unit of frequency, hertz is defined as the reciprocal of the SI unit of time, the second. The second has been defined as 1 s = $\frac{9192631770}{\Delta\nu_{Cs}}$, where $\Delta\nu_{Cs}$ is the unperturbed ground-state hyperfine transition frequency of the caesium-133 atom [26]. This transition frequency is by definition 9 912 631 770 Hz. All other frequencies are measured relative to this transition frequency. To use an atomic transition as an optical frequency reference a spectroscopic measurement must be made. There are many factors which can influence the accuracy of such a measurement. The Lorentzian linewidth of an atomic transition with radiative decay rate Γ and saturation intensity I_{sat} has a full width at half maximum of

$$\Delta\omega_{FWHM} = \Gamma\left(1 + \frac{I}{I_{sat}}\right)^{1/2}., \tag{2.3.1}$$

as given by Foot [5]. In equation 2.3.1 the effect known as power broadening can be observed due to the $\frac{I}{I_{sat}}$ term. Another commonly encountered broadening mechanism is Doppler broadening. The atoms in a vapour sample at a temperature above 0 K will possess a distribution of velocities. This means that the atoms will experience a Doppler shift of the laser frequency. Since not all atoms experience the same Doppler shift due to their distribution of velocities, this does not only cause a shift in the transition frequency, but a broadening of the spectral line. Doppler-free spectroscopic techniques such as saturated absorption spectroscopy can be used to counteract the Doppler broadening. Despite atomic transitions being the most accurate frequency references, spectroscopy as a laser frequency referencing technique suffer from the relatively high laser power required and that a transition at the desired laser frequency might not be accessible.

If the difference between two optical frequencies is small enough that it can be measured with relative ease, a laser can be used as an optical frequency reference for stabilising another laser. For the optical electric fields $E_1(t) = E_1 e^{i2\pi\nu_1 t}$ and $E_2(t) = E_2 e^{i2\pi\nu_2 t}$ produced by two lasers, if the two lasers are simultaneously incident on a photodetector the beat frequency $\nu_{beat} = |\nu_2 - \nu_1|$ can be extracted via electronic means provided that ν_{beat} is within the detector bandwidth [2]. The electronic signal can then be used to determine the frequency

[2] Photodetectors can have bandwidths in excess of 100 GHz [27].

difference between the lasers for stabilization.

For the most demanding frequency stabilized laser applications, such as sub-hertz laser linewidths for optical clocks, ultra stable optical reference cavities are used with the Pound-Drever-Hall technique used to generate the error signal [28]. This is the technique used in this project and is described in the following section.

2.3.2 Fabry-Pérot Cavities as Optical Frequency References

A Fabry-Pérot cavity consist of 2 mirrors separated by a medium of length l and refractive index n. This gives the cavity an optical path length $L = nl$. Such a cavity has a series of equally spaced resonance frequencies with the q'th resonance frequency determined by

$$\nu_q = \frac{qc}{2L} \tag{2.3.2}$$

and the separation between two adjacent resonance frequencies is known as the free spectral range and is given by

$$\nu_{FSR} = \frac{c}{2L} \tag{2.3.3}$$

where c is the speed of light in vacuum. Note that only the Gaussian (TEM_{00}) mode is considered in this section. A lossless cavity with mirror reflectances R_1 and R_2 has a finesse of

$$\mathcal{F} = \frac{\pi}{|\ln(\sqrt{R_1 R_2})|} \tag{2.3.4}$$

and linewidth

$$\delta\nu = \frac{\nu_{FSR}}{\mathcal{F}}. \tag{2.3.5}$$

This linewidth is the full-width at half maximum value of the Lorentzian lineshape of the cavity transmission/reflection [29].

Fabry-Pérot cavities can be used as frequency references for laser frequency stabilization, with the error signal being determined from the transmitted or reflected intensity as a function of laser frequency detuning from cavity resonance. Due to the optical path length dependence of the resonance frequencies, the stability of the frequency reference can be influenced by environmental conditions such as vibrations, pressure fluctuations and temperature changes. The

vibrations cause deformations of the cavity spacer which changes the distance between the cavity mirrors.

The dependence of the refractive index of air on temperature T in °C and pressure P in Pascal is described by the revised Edlén equation

$$(n-1)_{tp} = \frac{(n-1)_s P[1 + (0.601 - 0.00972T)P \times 10^{-8}]}{96095.43(1 + 0.0036610T)} \tag{2.3.6}$$

where $(n-1)_s$ is the chromatic dispersion of air for a given wavelength λ which is given by the equation

$$(n-1)_s = \left(8343.05 + \frac{2406294}{130 - (\lambda \times 10^6)^2} + \frac{15999}{38.9 - (\lambda \times 10^6)^2}\right) \times 10^{-8} \tag{2.3.7}$$

as given by Birch and Downs [30].

Due to thermal expansion of the cavity spacer, the q'th resonance frequency of the cavity changes with small temperature change ΔT by

$$\Delta\nu_q \approx -\alpha_L \nu_q \Delta T, \tag{2.3.8}$$

where α_L is the linear thermal expansion coefficient (CTE) of the cavity spacer. In principle α_L and the refractive index of air are temperature dependent, but for small changes in temperature these values are approximately constant.

To mitigate the impact of these environmental factors on the stability of the laser, the reference cavity must be designed such as to minimize the effect of these factors on the optical path length of the cavity.

The effects of a 1°C temperature increase on the resonance frequencies of a 10 cm cavity made from various commonly used spacer materials are shown in table 2.1. A commonly used spacer material not shown in table 2.1 is ULE®, which is a ceramic with a zero-crossing in its CTE at a particular temperature [31]. This zero-crossing allows for a very low CTE when the cavity spacer is held at this specific temperature. Invar was used as the spacer material for the cavities constructed for this project. The reasons for choosing Invar are discussed in section 4.3.

2.3.3 Pound-Drever-Hall Error Signal

The Pound-Drever-Hall (PDH) technique is a method for frequency stabilizing a laser to a reference cavity first implemented by Drever *et al.* [33]. The technique requires the phase modulation with angular frequency Ω and modulation

Table 2.1: Thermal expansion effects of 10 cm cavity with 1 °C increase at 20 °C. α_L values from Paquin [32].

Material	$\boldsymbol{\alpha_L}$ **[$\times 10^{-6}$K^{-1}]**	**ΔL [μm]**	**$\lvert\Delta\nu_1\rvert$ [MHz]**
Stainless Steel: 304	14.7	1.47	4400
Invar-36	1	0.1	300
Fused Silica	0.5	0.05	150
ZERODUR® Expansion Class 1	0.05	0.005	15

depth[3] β of a laser with carrier angular frequency ω. With the assumption that $\beta < 1$ the electric field incident on the cavity can be considered to consist exclusively of a carrier frequency with two first order sidebands as

$$E_i(t) = E_0 e^{i\omega t + i\beta \sin(\Omega t)} \approx E_0 \left(J_0(\beta) e^{i\omega t} + J_1(\beta) e^{i(\omega+\Omega)t} - J_1(\beta) e^{i(\omega-\Omega)t} \right), \tag{2.3.9}$$

where $J_n(\beta)$ are Bessel functions of the first kind. The electric field reflected off the cavity is obtained by applying the reflection transfer function to the incident field

$$E_i(t) = E_0 \left(R(\omega) J_0(\beta) e^{i\omega t} + R(\omega+\Omega) J_1(\beta) e^{i(\omega+\Omega)t} - R(\omega-\Omega) J_1(\beta) e^{i(\omega-\Omega)t} \right). \tag{2.3.10}$$

where

$$R(\omega) = \frac{r\left(e^{i\frac{\omega}{\nu_{FSR}}} - 1\right)}{1 - r^2 e^{i\frac{\omega}{\nu_{FSR}}}} \tag{2.3.11}$$

is the reflection transfer function for a lossless symmetric cavity with reflection coefficient r. Detecting the reflected power with a fast photodetector and demodulating the signal at Ω with an appropriate phase shift and then filtering out all oscillating terms yields the error signal as a function of the frequency detuning of the laser from cavity resonance. The error signal can be used in a feedback loop to minimize the laser frequency deviation form the cavity resonance. This signal can be separated into two regimes, namely the fast modulation $\Omega \gg \delta\nu$ and the slow modulation $\Omega \ll \delta\nu$ regimes. These regimes will be referred to as the PDH and the dithering regimes respectively for the remainder of this document[4]. The equations for these error signals are shown

[3]For phase modulation the modulation depth is equal to the peak phase deviation of the modulated signal.

[4]Sources differ on the nomenclature for these regimes. Black [34] refers to these as the fast and slow modulation regimes, Belfi *et al.* [35] refers to the dithering regime for the slow

in equations 2.3.12 and 2.3.13 where $P_c = |E_0|^2 J_0^2(\beta)$ and $P_s = |E_0|^2 J_1^2(\beta)$ are related to the powers in the carrier and each of the sidebands respectively [34]

$$\epsilon_{dither} \approx 2\sqrt{P_c P_s}\Omega \, \frac{d|R(\omega)|^2}{d\omega} \tag{2.3.12}$$

$$\epsilon_{PDH} \approx -2\sqrt{P_c P_s}\, \mathrm{Im}\{R(\omega)R^*(\omega+\Omega) - R^*(\omega)R(\omega-\Omega)\}. \tag{2.3.13}$$

The dithering regime requires in-phase demodulation and the PDH signal is demodulated in quadrature. The PDH error signal has the advantageous property of a steeper linear slope close to resonance over the dithering regime. Both signals possess a laser power independent locking point where the laser is resonant with the cavity. This has the advantage to the side-of-fringe[5] locking method that the frequency locking is decoupled from power fluctuations [34]. A plot of the two error signals for the same cavity is shown in figure 2.2. Close to resonance and for a high finesse cavity, the PDH error signal is a linear function of frequency detuning from resonance f as given by Black [34] to be

$$\epsilon_{PDH} \approx -8\frac{\sqrt{P_c P_s}}{\delta\nu} f. \tag{2.3.14}$$

The value of β which maximizes the slope of equation 2.3.14 is the value which maximizes $J_0(\beta)J_1(\beta)$. This value is $\beta = 1.08$ [34] [6].

2.3.4 Active Length Stabilization of an Optical Reference Cavity

Since the optical reference cavity provides a means to determine the frequency detuning from cavity resonance, the derived error signal can also be used to stabilize the optical path length of the cavity to a frequency stabilized laser. This is implemented by varying the cavity length by means of a piezoelectric actuator. Another laser can then be locked to the stabilized cavity, in effect

modulation. In their original paper Drever *et al.* [33] used the fast modulation regime to describe the technique.

[5] The side-of-fringe locking method uses the side of a reflected power fringe as the error signal.

[6] The assumption that $\beta < 1$ has been made in the derivation. This has been done to allow for the simplification in equation 2.3.9 that only the carrier and first order sidebands are considered. This has been done for mathematical simplicity. For $\beta > 1$ higher order sidebands must be included in equation 2.3.9. The optimum value of $\beta = 1.08$ will still be valid when second order sidebands are also considered in equation 2.3.9 [36].

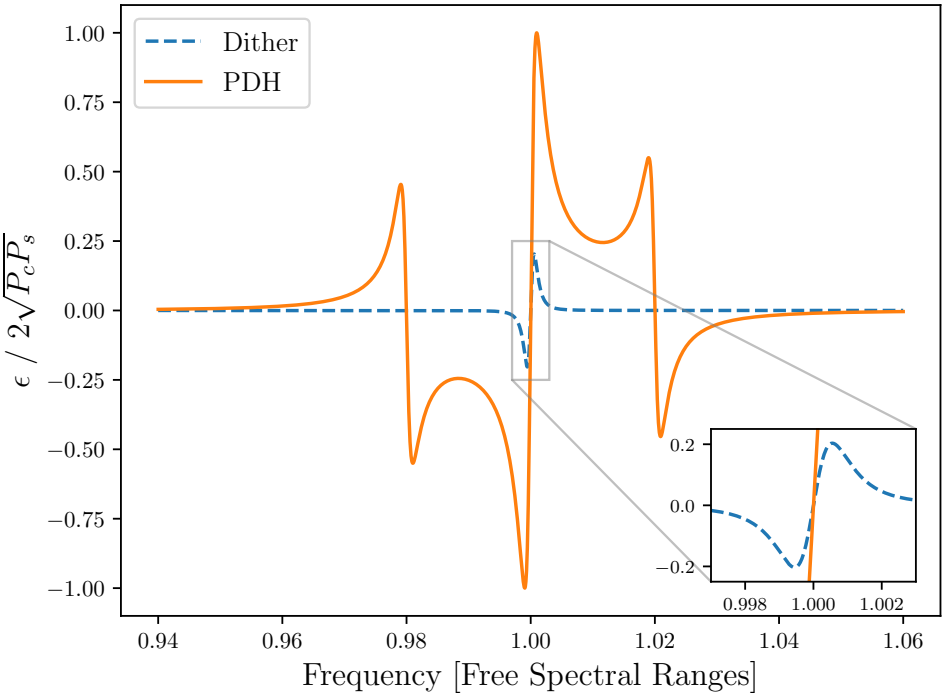

Figure 2.2: Simulated PDH and dithering error signals for a cavity with linewidth of 0.002 times the free spectral range. The PDH modulation frequency is 0.02 times the free spectral range and the dithering modulation frequency is 0.0003 times the free spectral range.

transferring the stability of the one laser to the other via the cavity [37]. Such a cavity is called a transfer cavity. This technique can be used to transfer the stability of the stable laser to multiple other lasers, provided the cavity mirrors are suitably reflective for all the wavelengths [38].

In the absence of a frequency stabilized laser, the reference cavity's optical path length can be stabilized by comparing an integer multiple of the cavity's free spectral range to the frequency separation of the carrier and a modulation sideband of the laser which is stabilized to the cavity. The cavity and hence laser stability is then limited by the stability of the modulation frequency. Defoe and Brewer [39] used a dual electro-optic modulation scheme to lock the laser to the cavity and to lock the cavity length using the modulation sideband. For the two modulation angular frequencies Ω and Θ with modulation depths α and β the incident electric field on the cavity is given by

$$E_i(t) = E_0 e^{i\omega t + i\alpha \sin(\Omega t) + i\beta \sin(\Theta t)}. \tag{2.3.15}$$

For this Ω is in the fast modulation regime and Θ is chosen such that $\Theta + \Omega$ is an integer multiple of the cavity free spectral range. The regular PDH error signal is obtained by demodulating with Ω and the error signal for the cavity length is obtained by demodulating with $\Theta + \Omega$.

A variation upon this method was used by Belfi *et al.* [35] to monitor the free spectral range of a ring laser gyroscope. The laser is phase modulated with angular frequencies Ω and Θ with modulation depths α and β with the Θ modulation frequency also frequency modulated with angular frequency ζ and frequency deviation γ. The Ω frequency is in the fast modulation regime, ζ is in the slow modulation regime and Θ is tuned to match an integer multiple of the free spectral range of the cavity. The error signal for the locking of the cavity length to a stable laser can be obtained by demodulating with Ω and demodulation at the frequency ζ produces an error signal for the monitoring of the free spectral range and hence the absolute length of the cavity.

Hagel *et al.* [40] used a piezoelectrically tunable Invar cavity which had its free spectral range locked to a stable radio frequency signal by injecting a frequency shifted beam in the opposite end of the cavity to reduce long term cavity resonance drifts to below 9 MHz per hour. The long term drift of the laser locked to the cavity without the cavity length feedback was 100 MHz/h. The frequency shift was produced using an acousto-optic modulator (AOM).

Chapter 3

Experimental Setup And Procedures

3.1 Laser Frequency Stabilization Setup

Before starting this project the stabilization of the 369 nm wavelength laser frequency was done in our laboratory using a spectroscopy measurement on a hollow cathode lamp. Due to reduced output power of the 369 nm wavelength laser it was no longer possible to perform the spectroscopy simultaneously with ion trapping. For this reason an alternative frequency stabilization system was required. The laser frequency stabilization method chosen to implement for this project was to use the Pound-Drever-Hall technique with in-house built optical reference cavities serving as the optical frequency references. A reference cavity was constructed for each of the two lasers. The two reference cavities' spacers were identical. In addition to these reference cavities a cavity with a different spacer design whose length can be tuned using a piezoelectric actuator was constructed for the 935 nm wavelength laser for experimenting with active length stabilization of an optical reference cavity.

The three cavity spacers were machined from a 2 inch diameter Invar rod. The distance between the mirrors for each of the fixed length cavities was 230 mm. The mirrors for the reference cavities were attached using Invar retaining rings. One of the mirrors for the tunable cavity was held in place with Invar retaining rings and the other mirror was glued to an Invar adapter which was glued to a piezoelectric actuator. The adapter was necessary since the piezo

must be glued on the face and the mirror in the side. The glue used was Torr Seal® and the piezo was a Noliac NAC2125-H06-A01. The mirrors for the reference cavities were custom coated with a specified reflectance of 99.7 % for the desired wavelength and 99.9 % for 935 nm for the tunable cavity. The mirrors were UV Fused Silica, plano-concave with diameters of 50 mm and radii of curvature of 1000 mm. The plane sides of the mirrors were anti-reflective coated for the requested laser wavelengths. A cross section of the tunable cavity is shown in figure 3.1.

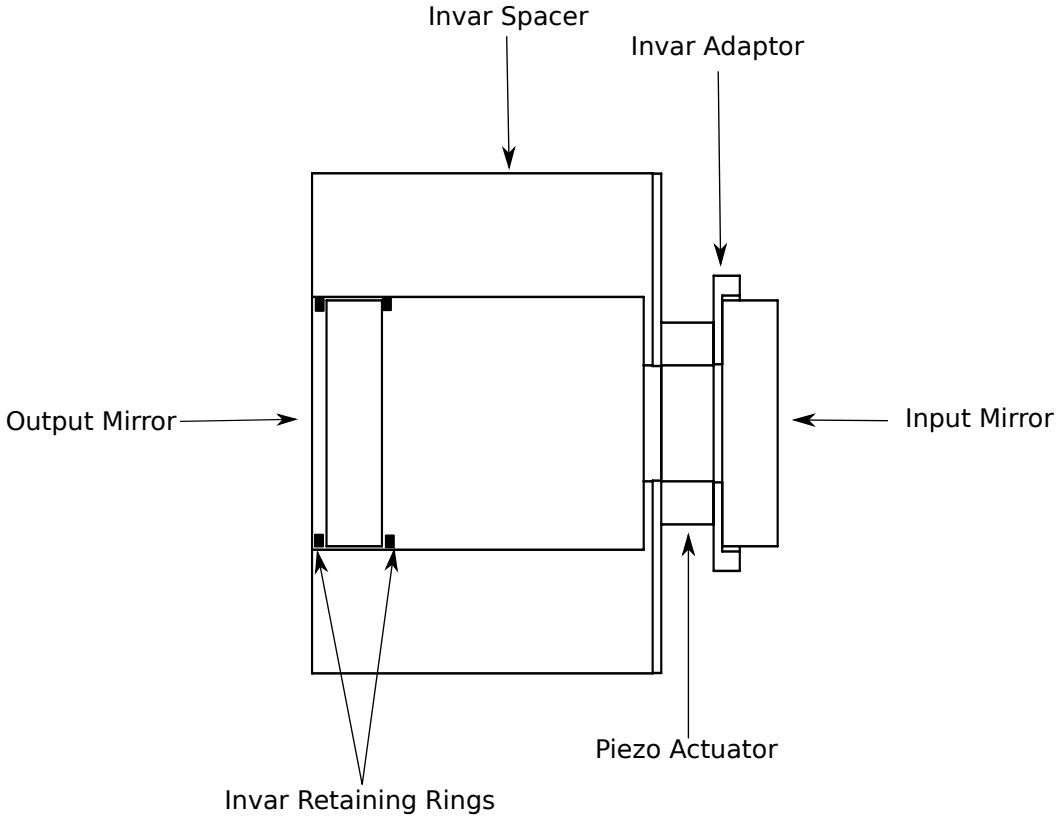

Figure 3.1: Cross section of the tunable cavity. Viewpoint perpendicular to the optical axis.

The cavities were placed on Polytetrafluoroethylene (PTFE) mounts inside a vacuum chamber. The points of contact of the reference cavities with the PTFE mounts were at the cavities' Airy points [1] as to minimize the angular deflection of the mirrors. The vacuum chamber had an electrical feedthrough

[1]The Airy points of a uniform rod are the two support points at which the ends of the rod exhibits zero angular deflection due to gravitational sagging [41].

for attaching the piezo to a driver. Six viewports allowed for light to travel through each of the cavities. The vacuum chamber was evacuated to a pressure in the range of mid 10^{-7} mbar using an Agilent Technologies SH-110 dry scroll vacuum pump and TwisTorr 84 FS turbomolecular pump. The pressure was monitored using an Adixen ACC 2009 cold cathode pirani gauge. The vacuum chamber was placed on a silicon mat and strapped to a vibration isolated optical table. A cross section of the cavities in the vacuum chamber is shown in figure 3.2. Drawings for the cavity spacers and PTFE mounts can be found in Appendix A. The vacuum chamber was temperature controlled

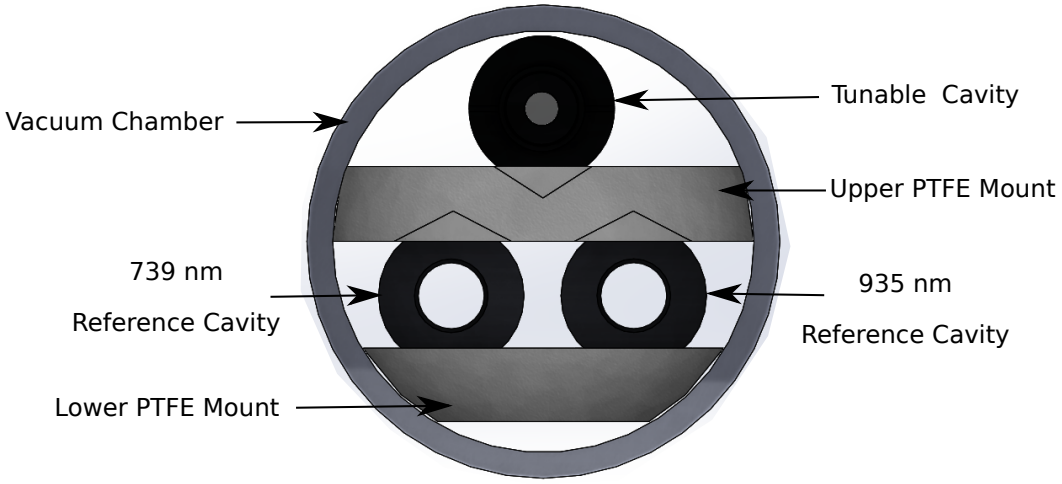

Figure 3.2: Cross section of the three cavities in the vacuum chamber. Viewpoint is from the incident end of the cavities.

using a Wavelength Electronics WTC3243 controller with its accompanying evaluation board. The controller powered two 5 W resistive heating pads to keep the chamber surface at approximately 32 °C. A Wavelength Electronics TCS10K5 10 kΩ thermistor was used to monitor the chamber surface temperature. The voltage across the thermistor was monitored on a computer with a USB DAQ to enable fine adjustment of the controllers proportional gain term and integral time constant to maximize the thermal stability of the vacuum chamber. Silicon and foam pads were wrapped around the vacuum chamber to provide thermal insulation.

The 739 nm wavelength laser was the seed laser of a Toptica TA-SHG Pro laser. The main output of the TA-SHG Pro is at 369 nm, the desired frequency for the ion trap. Both the 739 nm and 935 nm wavelength lasers had built-in

optical isolators. A simplified diagram of the setup for locking the 739 nm wavelength laser to the reference cavity is shown in figure 3.3.

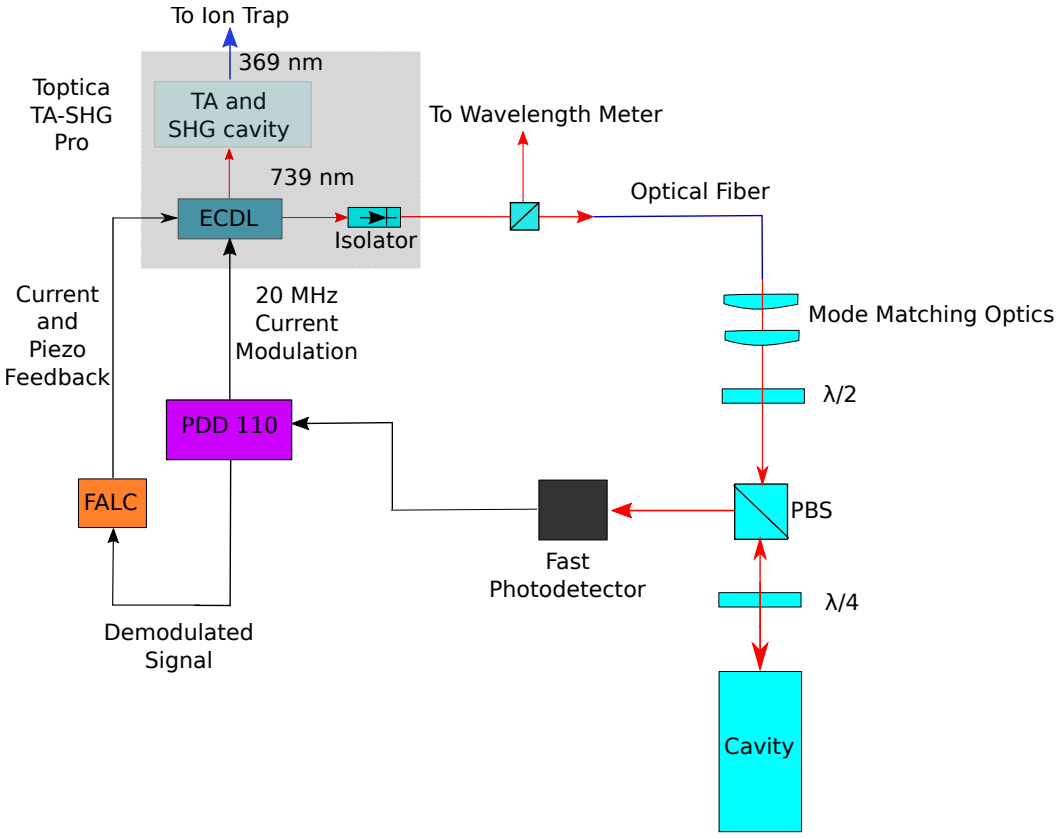

Figure 3.3: Simplified diagram of the setup for locking the 739 nm wavelength laser to the reference cavity. The symbols are described in the text.

One percent of the 739 nm wavelength laser output was tapped off before the tapered amplifier (TA) and frequency doubling (SHG) cavity. A beam-splitter was used to send 50% of the tapped off beam to a wavelength meter and the remainder sent through a polarization maintaining fiber optic patch cable. The patch cable served 2 purposes, directing the laser beam towards the reference cavities and cleaning the mode of the beam to simplify mode matching calculations. The output out of the fiber was sent through the following optics in sequence: mode matching lenses, half-wave plate ($\lambda/2$), polarizing beam splitter cube (PBS) and quarter-wave plate ($\lambda/4$) before being directed through the reference cavity. The back reflected beam passed though the quarter-wave plate and was diverted from the incident beam path using the beam splitter cube onto a reverse biased Thorlabs Det10 A/M photodetector.

The laser current was modulated using the 20 MHz signal provided by the Toptica PDD 110/Dual Pound-Drever-Hall detector module. The signal from the photodetector was demodulated and phase shifted by the PDD 110 to produce the PDH signal for locking the laser to the reference cavity. The Toptica Fast Analog Linewidth Control (FALC) 110 controller was used to complete the feedback loop. The main output of the FALC provided feedback to the laser current and the unlimited integrator output provided feedback to the laser's external cavity piezo. The main circuit branch of the FALC comprises of a series of lag-lead filter elements operating in different frequency regimes. The corner/cutt-off frequencies of the various filters can be adjusted to adjust the response of the controller output to the error signal.

A simplified diagram of the setup for locking the 935 nm wavelength laser to the reference cavity is shown in figure 3.4. The output of the Toptica DL

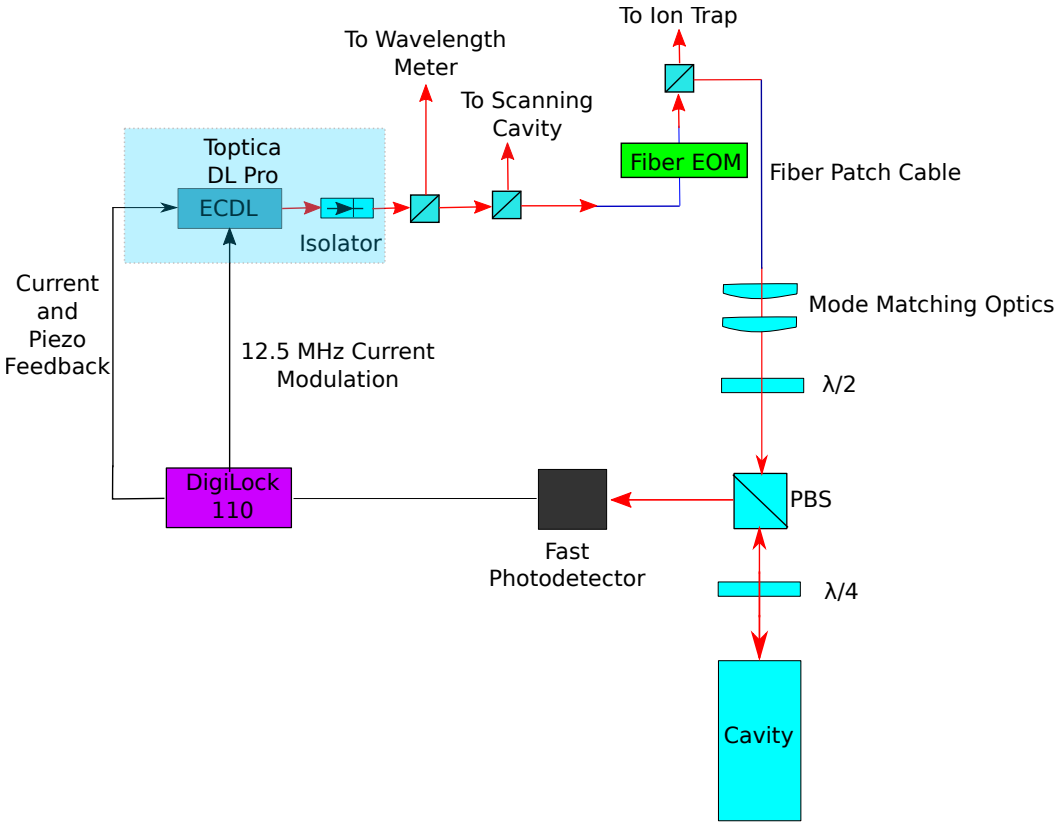

Figure 3.4: Simplified diagram of the setup for locking the 935 nm wavelength laser to the reference cavity. The symbols are described in the text.

Pro 935 nm wavelength laser was divided into 4 paths. A small fraction of the

output was sent to the wavelength meter, another small fraction was sent to a Thorlabs SA200-8B scanning Fabry-Perot cavity, the majority of the power was sent through a EOSPACE PM-0K5-10-PFA-935 fiber electro-optic modulator (EOM) towards the ion trap vacuum chamber. A fraction of the beam was tapped off after the EOM and sent through a polarization maintaining fiber optic patch cable towards the reference cavity. The optics between the fiber and the cavity were similar to that used for the 739 nm. The detector used was a New Focus 2107-FS-M with the adjustable gain set to 10X. The Toptica DigiLock 110 modulated the laser current with a 12.5 MHz signal and produced the PDH signal for locking the laser to the reference cavity. The DigiLock also served as the controller to provide current and piezo feedback to the laser.

The mode matching lenses used and their calculated positions, as measured from the output fiber coupler, are shown in tables 3.1 and 3.2. The position of the cavity is specified as the centre of the cavity, where the waist is formed. The positions of the lenses were determined by matching the incident beam waist to the cavity waist. More about mode matching a laser to an optical cavity can be found in Kogelnik and Li [42].

Table 3.1: Mode matching optics for 739 nm wavelength laser and reference cavity

Optical Element	**Property**	**Position [mm]**
Fiber Coupler	f = 11.16 mm	0
Mode Matching Lens 1	f = 500 mm	61
Mode Matching Lens 2	f = 200 mm	818
Cavity	waist radius = 0.27 mm	1392

Table 3.2: Mode matching optics for 935 nm wavelength laser and reference cavity

Optical Element	**Property**	**Position [mm]**
Fiber Coupler	f = 11.16 mm	0
Mode Matching Lens 1	f = 500 mm	61
Mode Matching Lens 2	f = 200 mm	817
Cavity	waist radius = 0.31 mm	1402

3.1.1 Laser Locking Procedure

The following procedure was performed to lock the lasers to the cavities:

1. The laser was roughly aligned through the cavity by overlapping the back reflections from the cavity.

2. The shape of the transmitted laser beam was monitored with a camera whilst the laser frequency was scanned. The steering mirror angles were adjusted until the TEM modes were visible.

3. Whilst scanning the laser frequency, the steering mirrors were adjusted to optimise the TEM_{00} mode power as detected with a power meter and monitored on an oscilloscope. The camera was used to identify the TEM_{00} mode. Since the cavity was not confocal, the TEM modes were non-degenerate.

4. An initial lock was performed with the controller.

   For the Digilock the laser scan range was lowered and the setpoint selected using the autolock function. After starting the feedback to the laser the scan was stopped automatically.

   For the FALC the scan range must be decreased manually whilst increasing the controller gain. The controller broadened the transmitted power lineshape as the controller attempted to keep the laser resonant with the cavity. This broadening indicates that the controller is working against the laser frequency scan and is not a physical broadening of the cavity transmission lineshape. As the scan range was decreased and the gain was increased progressively the transmitted power remained constant for the full scan range as the laser remained resonant with the cavity.

5. The stability of the laser was optimised by adjusting the controller parameters.

   For the Digilock this meant adjusting the controller gain and proportional, integral and derivative terms.

   For the FALC this constituted optimising the corner frequencies of the Slow Limited Integrator, Fast Limited Differentiator, Fast Limited Integrator and Extra Slow Limited Integrator as well as the Unlimited

Integrator speed. The Initial locking must be performed with the Extra Slow Limited Integrator and Unlimited Integrator disabled.

The transmitted power fluctuations and fluctuations of the error signal were used as measures of the quality of the lock. Further information on optimising the controller parameters can be found in the Digilock and FALC user manuals.

3.2 Cavity Characterization Setup

The free spectral ranges and linewidths of the cavities were measured by measuring the transmission peak separations and widths respectively. The lasers were locked to the cavities during the measurements. A simplified diagram of the setup can be found in figure 3.5. Modulation sidebands were generated using the fiber EOM. For the 739 nm the fiber EOM was attached to the fiber optic patch cable using a mating sleeve. The modulation frequency was generated by a R&S SMF100A frequency generator. A Thorlabs S120VC power meter was used to monitor the power transmitted through the cavity as the modulation frequency was scanned over a few megahertz either side of the cavity resonance. For the characterisation of the reference cavities the sideband frequency was scanned over the range 648 MHz to 654 MHz with a step width of 10 kHz and a dwell time of 3 milliseconds. RF levels of 1.1 V were used for the modulation signals. The frequency generator produced marker pules at the extremes of the scans. These marker pulses were used to calibrate the oscilloscope time scale to a sideband frequency scale. For the tunable cavity the sideband frequency was scanned from 4025 MHz to 4035 MHz. From the sideband frequency dependant transmission signals the free spectral ranges and linewidths were calculated.

3.3 Laser Frequency Noise Measurement Setup

The frequency noise power spectral densities of the lasers were measured by measuring the voltage noise power spectral densities of PDH error signals with the reference cavities serving as the optical frequency discriminators. For the 739 nm wavelength laser the PDH signal was the same as was used for locking

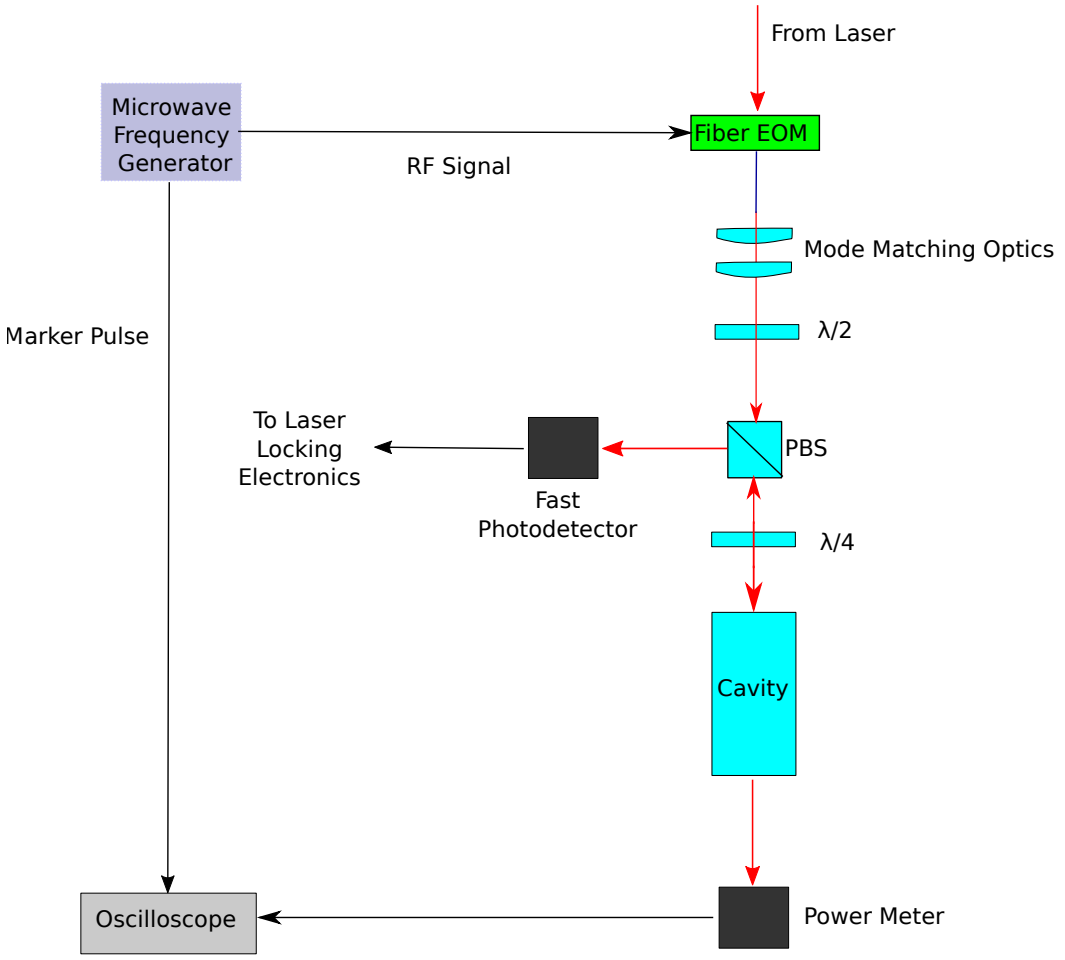

Figure 3.5: Simplified diagram of the setup for measuring the cavity linewidths and free spectral ranges. The laser locking electronics and optics before the EOM can be found in figures 3.3 and 3.4 for the 739 nm and 935 nm wavelength lasers respectively.

the laser to the reference cavity. The generation of this signal is shown in figure 3.3. This signal was accessed from the "monitor out" connector of the FALC. This PDH signal is analysed using the lock-in amplifier. The analysis process is described below.

The setup for the 935 nm wavelength laser is shown in figure 3.6. For the 935 nm wavelength laser an additional 20 MHz modulation of the laser current was applied. The 20 MHz signal was generated using the PDD 110 and the PDD 110 was also used as the demodulator for the generation of the PDH signal. The additional current modulation was required as the error signal for locking the laser to the cavity cannot be accessed from the Digilock for

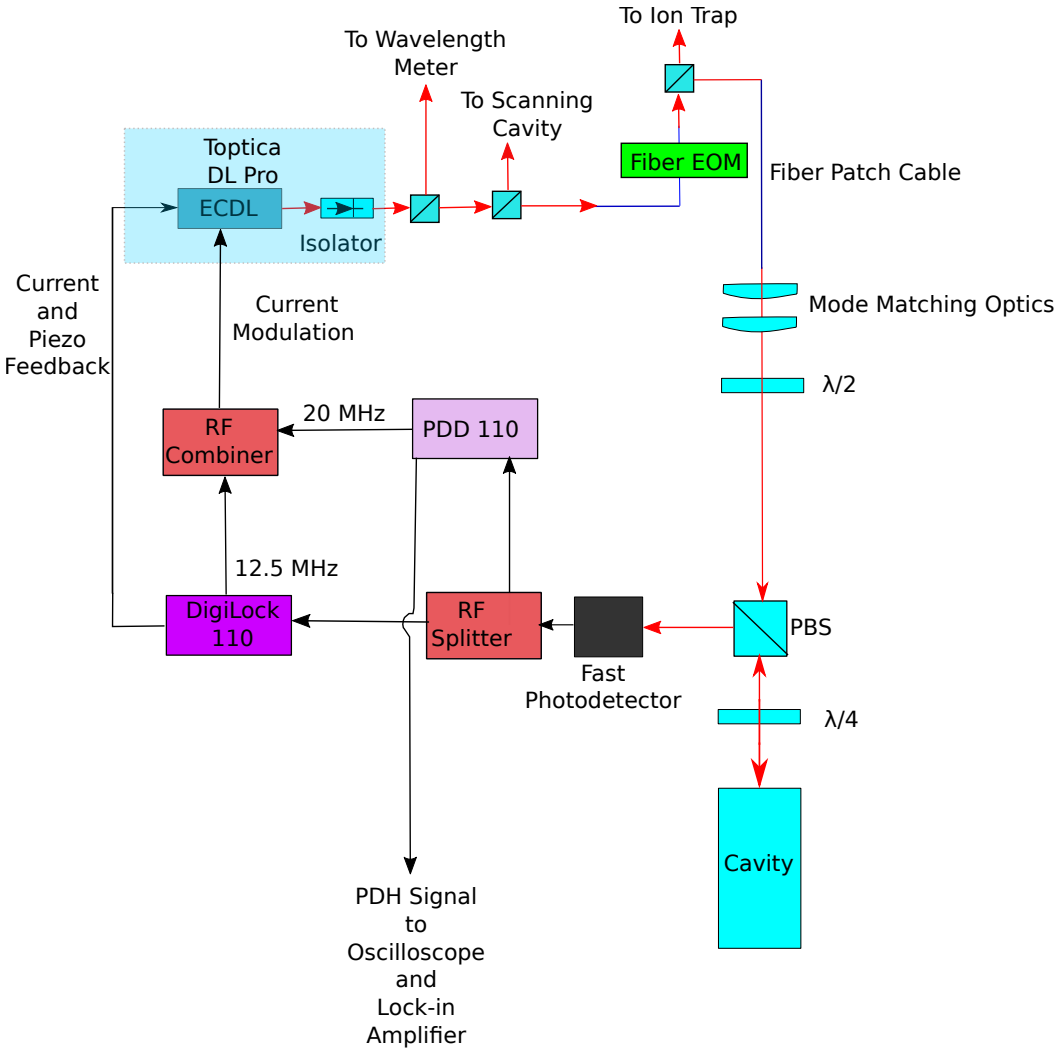

Figure 3.6: Simplified diagram of the setup for measuring the laser frequency noise of the 935 nm wavelength laser.

external analysis. The two modulation frequencies (12.5 MHz and 20 MHz) were combined with a Mini-Circuits ZFRSC-42+ RF power combiner. The signal from the photodetector which measures the 935 nm backreflection from the cavity was split in two paths using a RF power splitter. The one signal path was the same as used for locking the laser to the cavity. The other path was sent to the PDD 110 for demodulation using the 20 MHz signal.

These PDH signals were fed into the auxiliary input of a Zurich Instruments HF2LI lock-in amplifier. The voltage noise power spectral densities of the PDH signals were calculated by the HF2LI using a fast Fourier transform. The slopes of the PDH error signals were determined by scanning the laser

frequency over cavity resonance whilst monitoring the PDH error signals and the transmitted power on an oscilloscope. The PDH signals passed through a 1.9 MHz low pass filter to remove the oscillating components which are present due to the demodulation process. The oscilloscope time scale was converted to a laser frequency detuning from cavity resonance scale by using the known separation of the modulation sidebands from the carrier. This separation equals the modulation frequency. The slopes of the error signals provided a scaling from PDH signal voltage fluctuations to laser frequency fluctuations. This scaling was used to convert the voltage noise power spectral densities to laser frequency noise power spectral densities. The spectra were collected with the laser switched off to determine the detection noise and then collected with the laser on resonance with the cavity to determine the laser frequency noise. The measurements were performed with the lasers free running and locked to the reference cavities. The laser current and diode temperature were held constant across measurements for the same laser.

3.4 Laser Frequency Stability Measurement Setup

The long term frequency stability of the lasers were measured with a Bristol Instruments 621A wavelength meter with a sample rate of 4 Hz. The measurements were taken first with the lasers free running and then locked to the reference cavities. The measurement duration was 5 hours and performed with the laboratory vacant for noise reduction, except for the initial starting of the measurement after which the laboratory door was opened and closed to exit the laboratory. A temperature monitor was used to monitor the ambient temperature in the laboratory during the measurements.

3.5 Simultaneous Laser Frequency and Cavity Length Stabilization

The setup for the tunable cavity was similar to that used for the 935 nm lock to the reference cavity, except that the cavity and the mode matching optics were different and the output out of the EOM was sent directly to the locking

setup, not to the ion trap chamber. A simplified diagram of the setup for the tunable cavity locking is shown in figure 3.7. The mode matching optics are

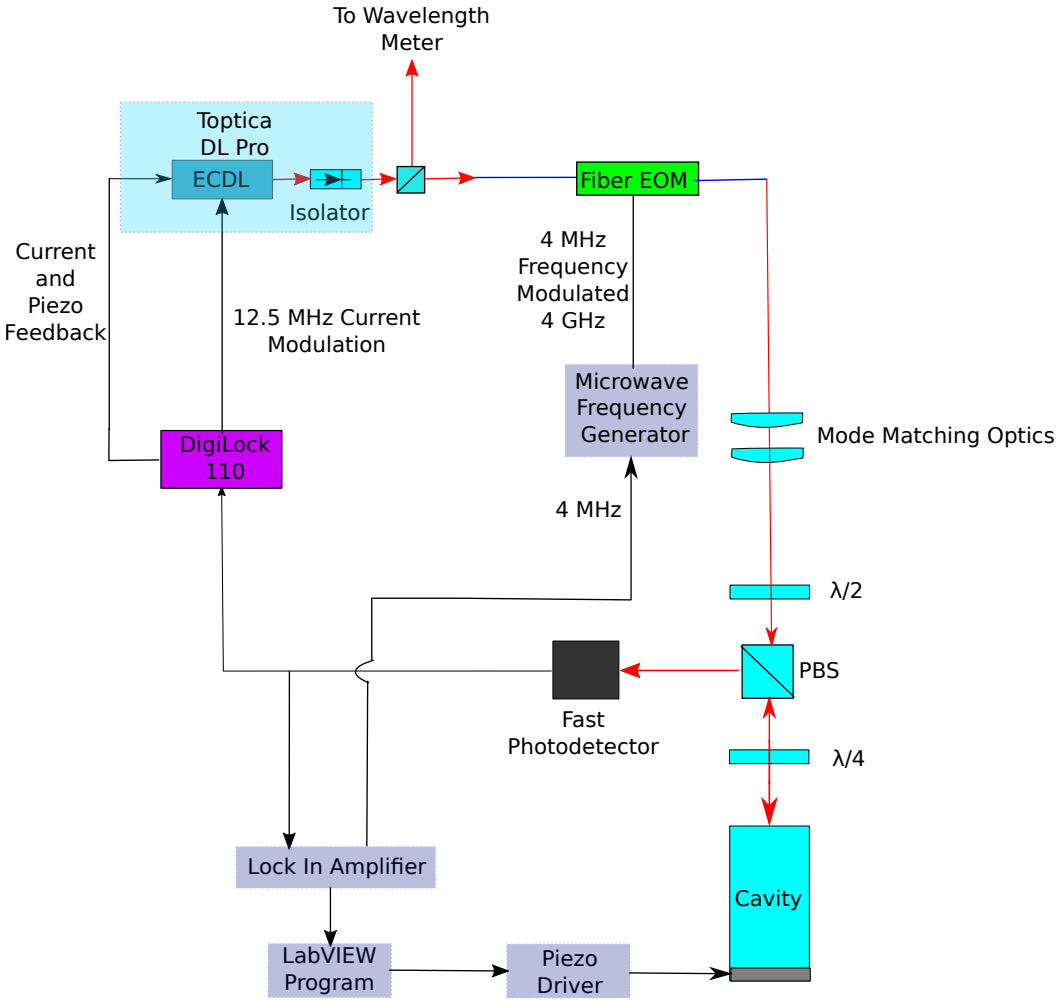

Figure 3.7: Simplified diagram of the setup for locking the 935 nm wavelength laser to the tunable cavity and simulation lock of the cavity free spectral range to a microwave frequency.

presented in table 3.3. An additional phase modulation with frequency matching the cavity free spectral range was applied to the laser using the EOM. The signal applied to the EOM was a 17 dBm [2] sinusoidal signal with a frequency of 4.0406 GHz generated by a R&S SMF100A microwave frequency generator. The microwave frequency generator can be referenced to a Stanford Research Systems FS725 Rubidium frequency standard to stabilize the 4 GHz frequency.

[2]The dBm scale expresses the ratio of the power value to 1 mW using the decibel scale.

Table 3.3: Mode matching optics for 935 nm wavelength laser and tunable cavity

Optical Element	Property	Position [mm]
Fiber Coupler	f = 11.16 mm	0
Mode Matching Lens 1	f = 125 mm	41
Mode Matching Lens 2	f = 100 mm	281
Cavity	waist radius = 0.2 mm	1024

A 4.144 MHz signal generated by a Zurich Instruments HF2LI lock-in amplifier was used as a frequency modulation with a 4.476 MHz frequency deviation applied to the microwave frequency generator signal. The modulation index of the 4 MHz frequency modulation was 1.08 [3]. The signal from the photodector was split into two paths using a Mini-Circuits ZFSC-2-4+ power splitter. One path was used as the input for the Digilock for demodulation at 12.5 MHz for locking the laser to the cavity. The other path passed through a Mini-Circuits BLP-5+ DC-5 MHz low pass filter to attenuate the 12.5 MHz signal. After the filter the signal was amplified with a Mini-Circuits ZFL-500LN+ 27 dB amplifier. The HF2LI lock-in amplifier demodulated the amplifier output with the 4.144 MHz frequency modulation signal in-phase. A 973 mHz low pass filter was used in the demodulation path of the lock-in amplifier. The amplitude of this demodulated signal was the error signal for the cavity length lock. The slope of the error signal was determined by scanning the 4 GHz frequency produced by the microwave frequency generator from 4.030390 GHz to 4.030890 GHz using a sawtooth sweep with a step linearity of 250 Hz whilst the laser was locked to the cavity and recording the lock-in amplifier demodulated signal on an oscilloscope. The error signal was used as input signal for a LabVIEW feedback loop. The LabVIEW program sampled the demodulated signal at 225 samples per second and performed a 10 second average of these values. A Synertronic Designs Sveta 50V1LN ultra low noise piezo driver was used to drive the piezo. This driver was also controlled using LabVIEW. The design of the piezo driver was commissioned for this experiment. The low noise (120 nV_{pp}) was possible at the compromise of lower maximum output (55 V) and slow feedback bandwidth (0.024 s time constant).

The errors signals for the simultaneous locking of the laser to the cavity and

[3]For single tone frequency modulation with modulation frequency f and frequency deviation Δf the modulation index is given by $\frac{\Delta f}{f}$.

the cavity length to a modulation sideband of the laser are derived in appendix B. Numerical investigations of these signals were performed using Python. The results of the numerical simulations can also be found in appendix B with the code included in appendix C. The results of the numerical investigations informed the modulation parameters used in the experimental setup.

Chapter 4

Results and Discussion

4.1 Cavity Characterization

To determine the cavities' linewidths and free spectral ranges, modulation sidebands were scanned over cavity resonance whilst monitoring the transmitted power through the cavity. These sidebands were generated by applying a phase modulation to the lasers using the fiber EOM as discussed in section 3.2. The sidebands were scanned by scanning the modulation frequency generated by the microwave frequency generator. The lasers were locked to the cavities during these measurements and the modulation frequencies were chosen such that they were scanned over the next resonance frequencies from where the lasers were locked to. Lorentzian functions were fitted to the cavity transmission lineshapes obtained from scanning the modulation frequency generated by the microwave frequency generator. The fitting function used was

$$y = a\frac{\gamma}{(x - x_0) * *2 + \gamma^2} + y_0 \tag{4.1.1}$$

and the fitting algorithm uses a non-linear least squares method. This function is centred at x_0 and has a full width at half maximum value of 2γ. Five measurements were performed with each of the cavities. An example fit for the 739 nm can be found in figure 4.1, in figure 4.2 for the 935 nm wavelength reference cavity and in figure 4.3 for the 935 nm wavelength tunable cavity. The fitting parameters for these three example fits are shown in table 4.2.

The centre of the Lorentzian is the free spectral range of the cavity and the full width at half maximum value of the Lorentzian is the linewidth of the cavity for sufficiently narrow laser linewidth. The ratio of the free spectral

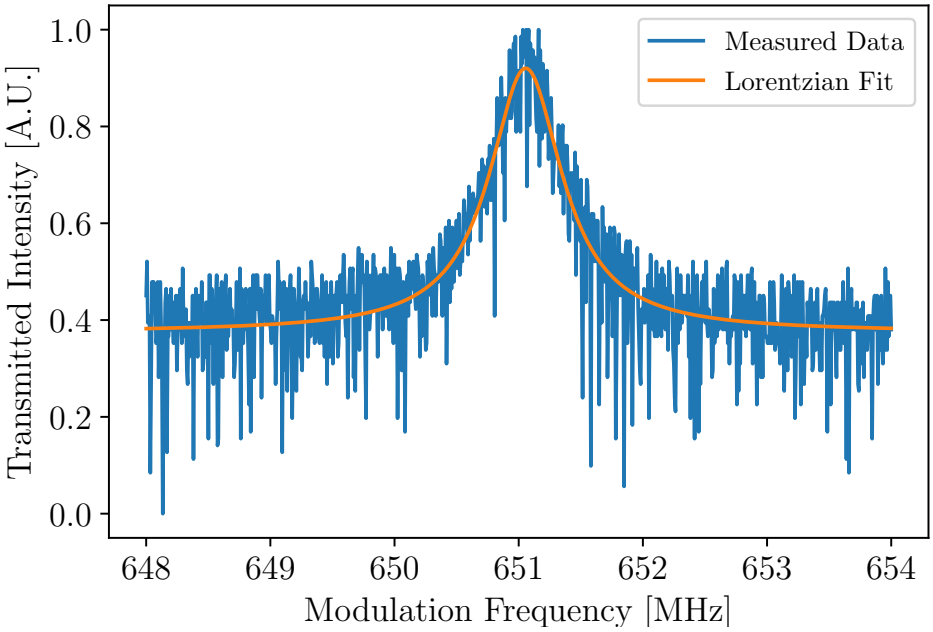

Figure 4.1: Cavity transmission with scanning modulation frequency for 739 nm wavelength with Lorentzian fit ($R^2 = 0.73$).

Table 4.1: Example fitting parameters. Uncertainty reported as standard error as determined from the square root of the diagonal covariance matrix values. Fitting parameter labels are shown in equation 4.1.1

Cavity	**a**	γ	$\mathbf{x_0}$	$\mathbf{y_0}$
739 nm Reference	0.196 ± 0.007	0.36 ± 0.01	651.056 ± 0.008	0.375 ± 0.004
935 nm Reference	0.197 ± 0.003	0.267 ± 0.005	651.188 ± 0.003	0.156 ± 0.002
935 nm Tunable	0.450 ± 0.009	0.56 ± 0.01	4030.662 ± 0.008	0.174 ± 0.003

range and the linewidth is the finesse of the cavity, as shown by equation 2.3.5. The reflectance of the mirrors for two identical mirrors can be calculated from the finesse using equation 2.3.4. The measured cavity properties can be found in table 4.2. The reported values are the averages from the five measurements with the uncertainty reported as the standard error across these measurements. Only the statistical uncertainties were calculated for the results presented in this section. If the error estimates needs to be improved for other purposes the systematic uncertainty must also be estimated. The analysis assumes that the laser has an infinitely narrow linewidth. As the lasers have finite linewidths the measured cavity linewidths will be broader than the actual cavity linewidth, but for sufficiently narrow laser linewidths this influence is negligible. The error

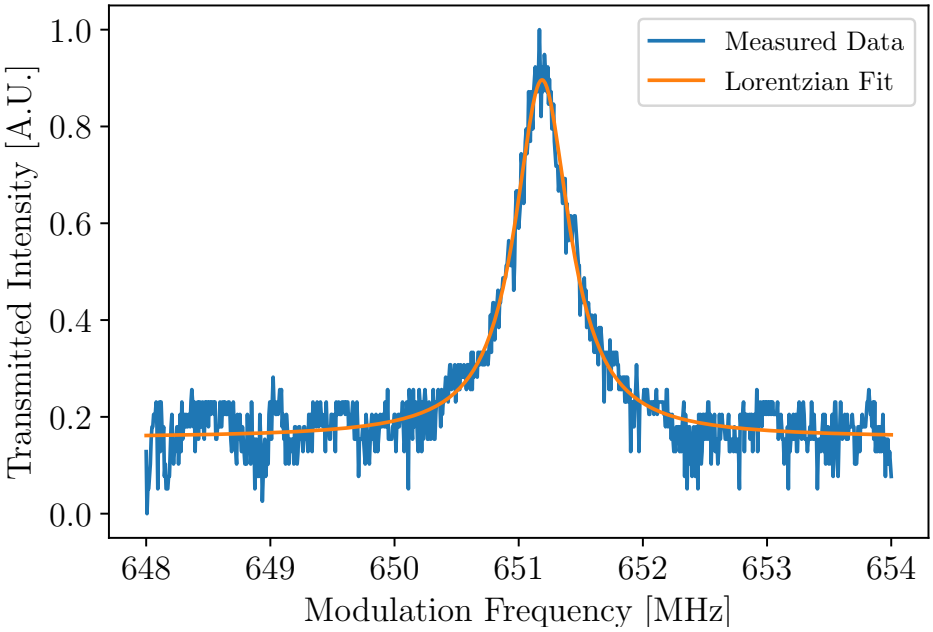

Figure 4.2: Cavity transmission with scanning modulation frequency for 935 nm wavelength reference cavity with Lorentzian fit ($R^2 = 0.94$).

estimates used were deemed sufficient for the purposes of the measurements.

Table 4.2: Measured cavity properties from scanning modulation sideband measurements. Uncertainty reported as standard error over 5 measurements.

Cavity	**Free Spectral Range [MHz]**	**Length [mm]**	**Linewidth [kHz]**	**Finesse**	**Reflectance [%]**
739 nm Reference	651.061 ± 0.002	230.234 ± 0.001	780 ± 20	830 ± 20	99.622 ± 0.009
935 nm Reference	651.191 ± 0.004	230.188 ± 0.002	537 ± 6	1200 ± 10	99.741 ± 0.002
935 nm Tunable	4030.67 ± 0.01	37.1889 ± 0.0001	1140 ± 70	3600 ± 200	99.911 ± 0.005

The additional noise present in the measurements of the 739 nm wavelength laser cavity transmission signal, which were not present in the 935 nm wavelength reference cavity measurements arises from instabilities in the laser lock. This was due to the attenuation of the 739 nm wavelength laser though the fiber EOM. The power out of the EOM was 14 μW compared to the power out of the patch cable of 576 μW. The attenuation was likely caused by losses at the fiber coupling sleeve, misalignment of polarisation maintaining axes of the fibres and attenuation in the fiber of the EOM, since the EOM was not designed to function at that wavelength. The low laser power necessitated

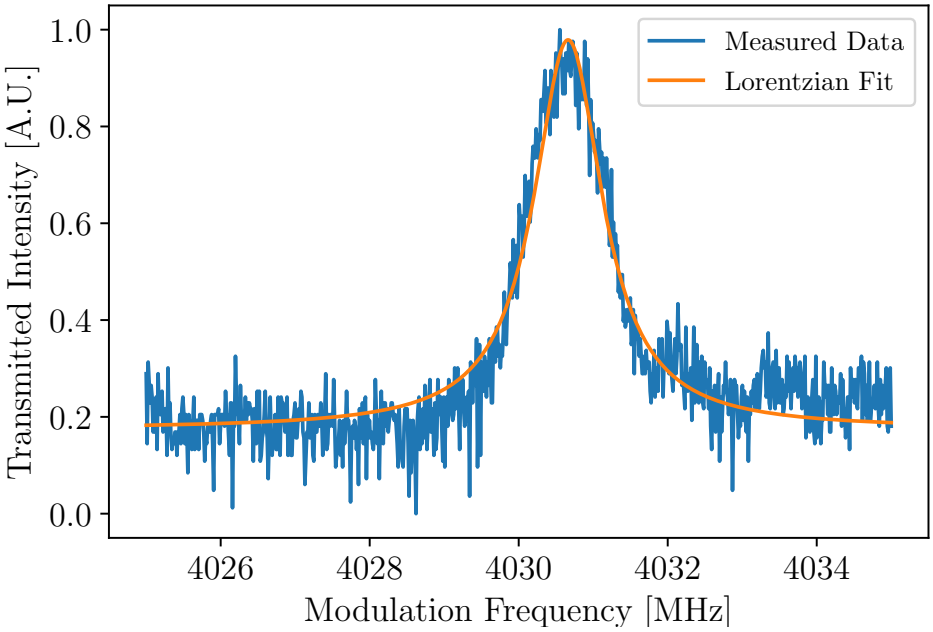

Figure 4.3: Cavity transmission with scanning modulation frequency for 935 nm wavelength tunable cavity with Lorentzian fit ($R^2 = 0.91$).

amplification of the error signal which resulted in the lock instabilities due to the noise from the amplification.

The manufacturer specified reflectances of the mirrors for the reference cavities were 99.7 ± 0.1 % and 99.90 ± 0.05 % for the mirrors used in the tunable cavity. The measured reflectances were within these specifications. This means that no significant damage was done to the mirrors or contaminants left on the mirror surfaces during installation.

The linewidth of the cavity can also be measured by scanning the free-running laser frequency over the cavity resonance whilst monitoring the transmitted power. The scanning is performed by varying the laser piezo voltage. The scanning rate used is a trade off between the cavity storage time and laser linewidth, as the transmitted power is the convolution of the laser and cavity linewidths. For slow scan speeds the low frequency noise of the laser increases the laser linewidth which broadens the measured transmitted power lineshape. For fast scan speeds the laser is not resonant with the cavity for a sufficient time for the electric field inside the cavity to reach steady state. An example result from scanning the free running 739 nm wavelength laser over

the reference cavity resonance is shown in figure 4.4. An estimated scan rate

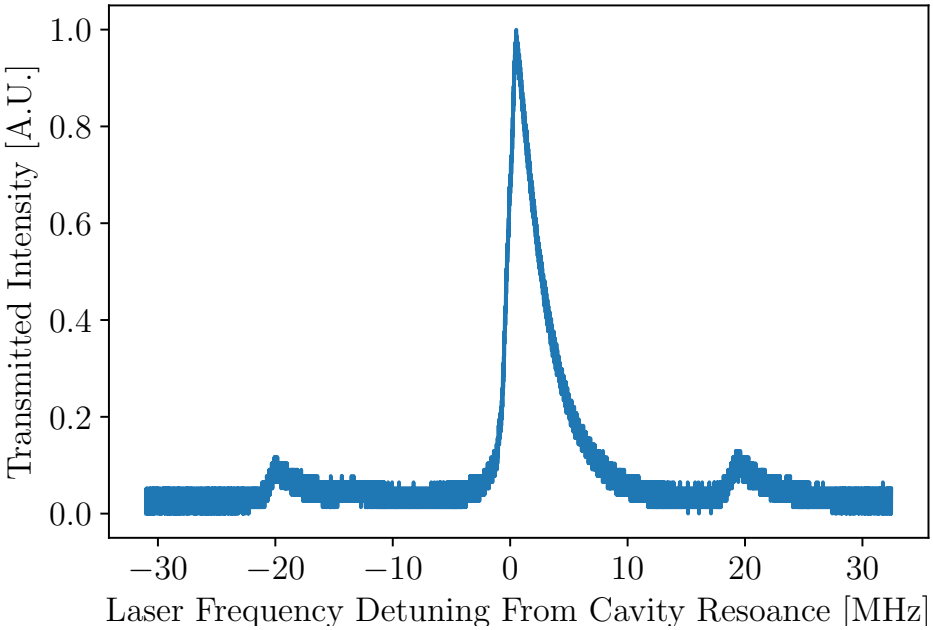

Figure 4.4: Reference cavity transmission with 739 nm wavelength laser frequency scanned by scanning the laser piezo voltage.

of 400 GHz/s was used. The 20 MHz modulation side-bands are visible as the secondary peaks in the figure and have been used to scale the horizontal axis. The asymmetry of the profile is due to the relatively fast laser frequency scan rate. Slower scan rates yielded variations across different scans due to variance in the laser frequency. A full description of the effects of scan speed and laser linewidth on the coupling into optical cavities is derived by Morville *et al.* [43].

The reason for the method of scanning the modulation frequency applied to the EOM was the lasers were locked to the cavities, the frequency noise of the lasers should be reduced and become negligible compared to the cavity linewidths when fitting the Lorentzians to the cavity transmission signals. Therefore the scanning modulation frequency yields a more accurate measurement of the cavity linewidth than if the free running laser frequency was scanned over the cavity resonance.

An alternative method to measure the cavity finesse is to perform a ring-down measurement. Such a measurement would use an acousto-optic modula-

tor as a beam deflectors to quickly turn off the light sent to the cavity whilst the laser is locked to the cavity. The decay constant of the light in the cavity could be used to determine the finesse of the cavity. This measurement was not performed as it does not yield the free spectral ranges of the cavities and other measurements similar to the ones performed would be required to get accurate measures of the free spectral ranges.

4.2 Laser Frequency Noise

The frequency noise of the lasers were determined by measuring the voltage noise of PDH error signals. The setup for these measurements is described in section 3.3. The slopes of the PDH signals used to determine the laser frequency noise were determined as follows: The laser frequency was scanned over the reference cavity resonance by applying a triangular voltage ramp to the laser piezo whilst monitoring the power transmitted through the cavity and the 20 MHz demodulated PDH signal with a low pas filter on an oscilloscope. These signals are shown in figure 4.5a for the 739 nm wavelength laser and in figure 4.5b for the 935 nm wavelength laser. The signal magnitudes have been scaled for illustrative purposes. For the transmission signal for the 935 nm the 12.5 MHz modulation sidebands are also visible in figure 4.5b. The 20 MHz sidebands in the cavity transmission signal were used to calibrate the oscilloscope time scale to a laser frequency detuning from cavity resonance scale. Linear functions were fitted to the central slopes of the PDH signals. The slope of the PDH signal was determined to be 1.73 $\times 10^{-6}$ V/Hz for the 739 nm wavelength laser and 1.33 $\times 10^{-6}$ V/Hz for the 935 nm wavelength laser. The slopes provides a conversion from PDH error signal voltage changes to laser frequency changes. These slopes were used to convert the measured voltage noise power spectral densities to laser frequency noise power spectral densities. The laser frequency noise power spectral densities of the locked and free running 739 nm wavelength laser are shown in figure 4.6 and in figure 4.7 for the 935 nm wavelength laser. The displayed spectra are the averages of 10 measurements each. The measurement duration was 2.277 s and the measured spectra have resolutions of 439.2 mHz.

The numerical integration of equation 2.2.1 using Simpson's rule yields

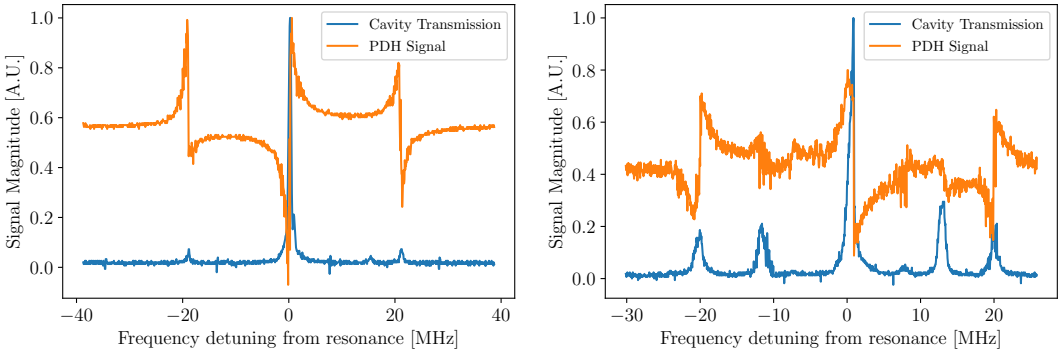

(a) (b)

Figure 4.5: PDH signals and Cavity transmission of laser frequency scanned over the resonance of the reference cavity for (a) 739 nm wavelength laser and (b) 935 nm wavelength laser.

the estimated linewidths for various observation times[1]. These linewidths are shown in table 4.3 with the average of the 10 spectra reported and the uncertainty reported as the standard error across the measurements.

Table 4.3: Laser linewidths as determined from numerical integration of the frequency noise power spectral densities. Reported values are the average over 10 measurements with the uncertainty reported as the standard error.

Laser	**Laser linewidth 1.138 s observation time [kHz]**	**Laser linewidth 0.1138 s observation time [kHz]**	**Laser linewidth 0.01138 s observation time [kHz]**
Free Running 739 nm	122 ± 9	120 ± 9	118 ± 9
Locked 739 nm	11.92 ± 0.07	12.03 ± 0.05	10.93 ± 0.04
Free Running 935 nm	110 ± 20	110 ± 20	100 ± 20
Locked 935 nm	5.4 ± 0.8	3.7 ± 0.5	3.2 ± 0.4

The PDH signal which is used to lock the laser to the cavity cannot be used to accurately determine the laser frequency noise independent of the cavity resonance frequency variations, since this signal does not distinguish between cavity resonance and laser frequency fluctuations. Using the same cavity to measure the laser frequency noise and to stabilize the laser frequency can only yield a lower bound on the laser linewidth, since the measurement

[1]The same spectrum was used for all the linewidth estimates. The different observation times were implemented by changing the lower bound of the integral. This has the same effect as measuring the spectra for the different times with different sampling rates to gave the same frequency resolution for all observation times.

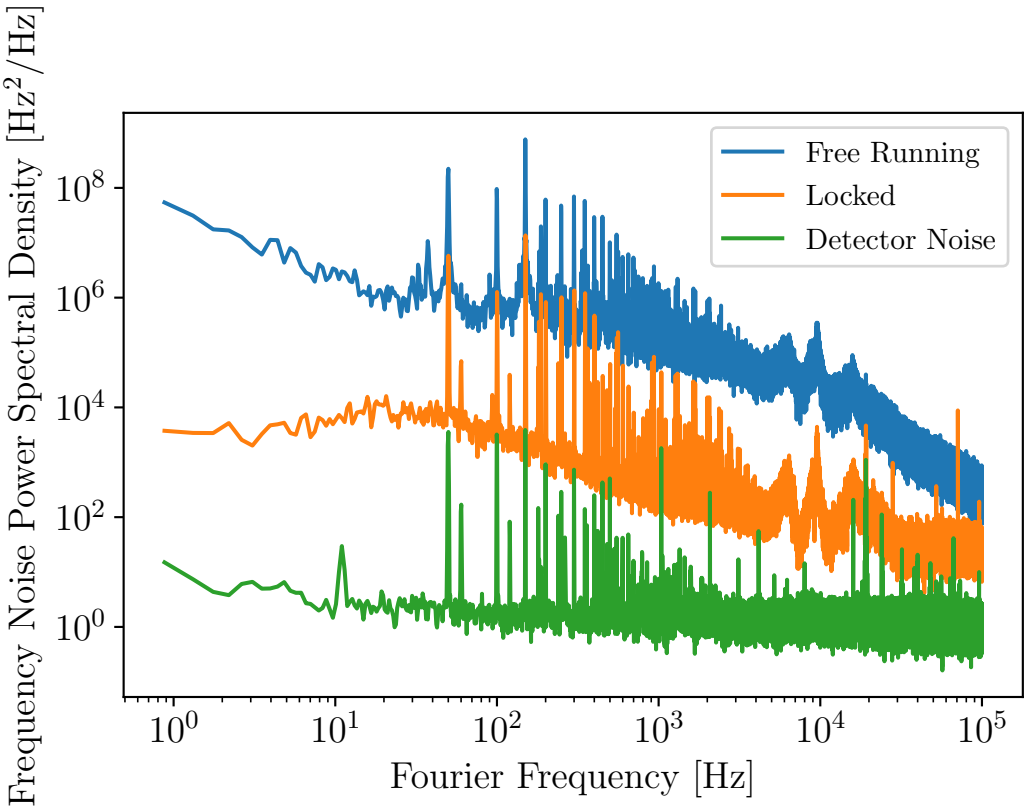

Figure 4.6: Measured 739 nm wavelength laser frequency noise power spectrum

and stabilization systems are not independent. Laser frequency noise which is not detected and hence not minimised by the stabilization system will also not be detected by the frequency noise measurement.

Low frequency noise has a dominant effect on the laser linewidth. This is explained by treating the frequency noise as a frequency modulation, with the modulation index scaling as $1/f$. For this reason seismic noise is a major contributor to the linewidth at long observation times. The cavities were not designed to minimize the effect of seismic noise. Examples of cavities designed to mitigate the effects of low frequency vibration can be found in Millo *et al.* [44]. The optical table's pneumatic stabilization system had a resonance at 1.5 Hz and provided amplification at these low seismic frequencies. If the vibration isolation performance of the cavities needs to be improved the vacuum chamber should be placed on breadboard with vibration isolators which are designed to damp these low frequencies. The turbomolecular pump is driven at a frequency of 1350 Hz. Due to the proximity of the vacuum pumps to the reference cavities

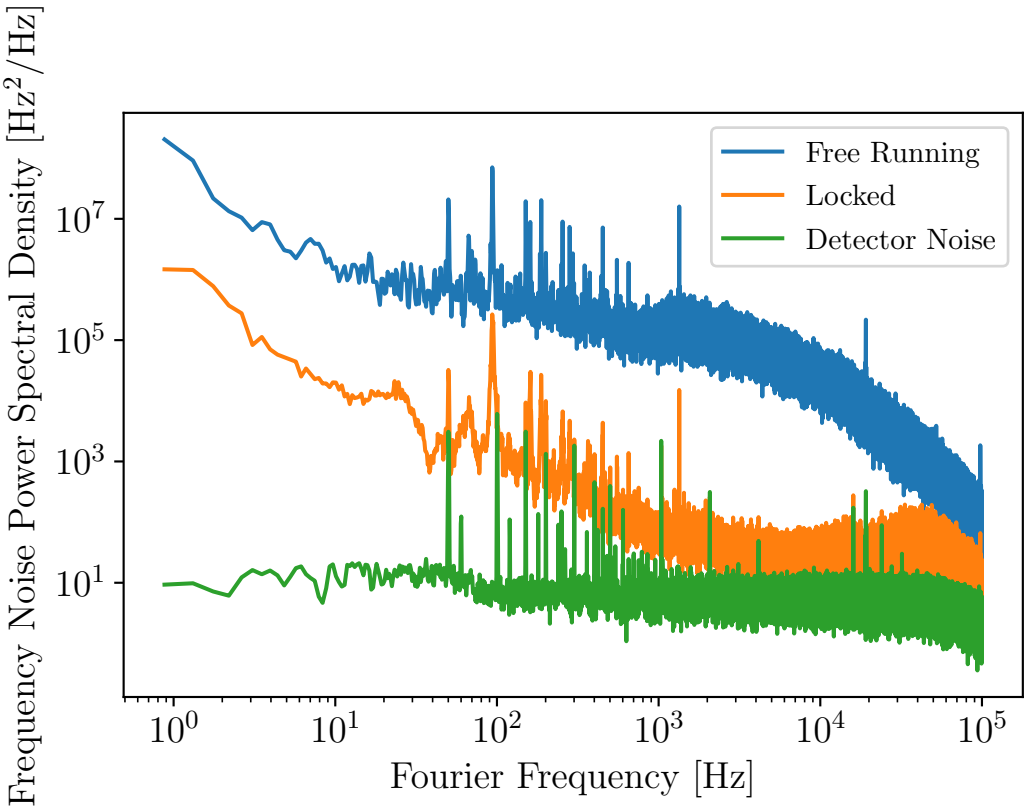

Figure 4.7: Measured 935 nm wavelength laser frequency noise power spectrum

the pumps are expected to be major contributors to the vibrations experienced by the cavities. These pumps should be exchanged for an ion pump to remove these vibrations. For the timescales over which the laser frequency noise was measured, the main contributions to the noise are expected to be vibrations of the laser cavity and reference cavity, piezo voltage noise and laser current noise.

The highest frequency present in the measured spectra is limited by the 100 kHz low pass filter of the auxiliary input of the lock in amplifier and the lowest frequency was chosen such that the estimated linewidth at 1 second observation time could be determined. Due to the dominance of the low frequency noise on the laser linewidth, higher frequency noise which could not be determined using this method will have a negligible effect on the linewidth for the long observation times of interest for this project.

For the 935 nm wavelength laser optical feedback from the back reflections off the cavity into the laser cavity was suspected to occur which destabilized

the laser frequency. This was investigated and could be observed when under the following conditions: The laser was operating stably, as observed with the wavelength meter, and non resonant with the cavity. If the beam was then blocked from reaching the cavity, a large jump in laser frequency was observed. After the frequency jump the laser frequency fluctuated greatly. When the block was then removed the laser returned to stable operation. This behaviour is shown in figure 4.8. The behaviour of the laser when blocked

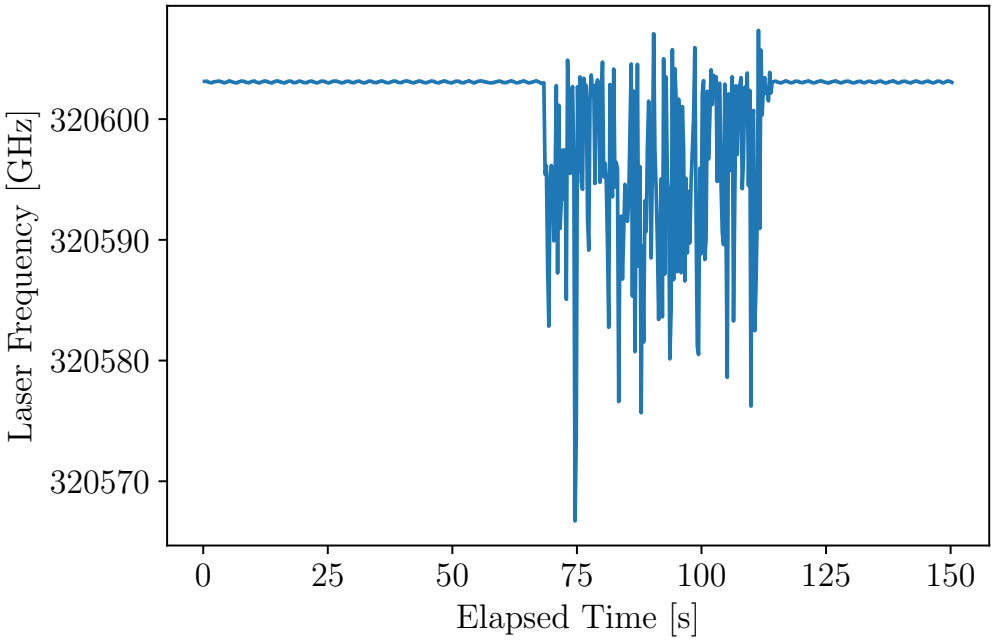

Figure 4.8: Frequency of the 935 nm wavelength laser when the light towards the cavity was unblocked, blocked and then unblocked again.

was typical of the laser operating in a multimode manner. Similar behaviour occurred if the laser was operating stably whilst the beam was blocked from reaching the cavity and then the block was removed. This indicated that the back reflected beam was providing optical feedback to the laser. Diode laser are very sensitive to external optical feedback. This is exploited in external cavity diode lasers as the optical feedback from the external grating is used to narrow the optical spectrum and to enhance the single mode tunability [45]. Unwanted optical feedback can influence the lasers intensity noise [46], current modulation response [46] and optical spectrum [47]. For a non impedance

matched cavity, some light will always be reflected even when a single frequency laser is resonant with the cavity. The PDH technique also relies on the complete back reflection of the modulation sidebands when the carrier is resonant with the cavity. The laser has an integrated optical isolator, but it is believed that the back reflections from the cavity was too great for the isolator to suppress to an acceptable level. It has been confirmed with the laser's manufacturer that the installed isolator is a 30 dB isolation model and that a 60 dB model is recommended if back reflections are expected to reach the laser cavity. To mitigate this effect the coupling efficiency into the fiber optic patch cable was intentionally reduced by misalignment of the fiber coupler. This reduced the optical power incident on the cavity and hence back reflected into the laser cavity. This decreases the slope of the PDH signal, limiting the possible stability of the laser due to reduced signal to noise ratio of the PDH signal voltage. The measurements were performed with the intentional misalignment. To eliminate this an additional optical isolator must be purchased and inserted in the beam line. With sufficient isolation the laser power sent to the reference cavity can be increased. Increased laser power will improve the slope of the PDH error signal and hence the possible frequency stability of the laser. The locations where the laser beams were tapped off towards the reference cavities were chosen such as to minimize the effect on the setups already present on the optical table. For the 739 nm the only effect is that the power sent to the wavelength meter had reduced. The power sent to the wavelength meter was still more than required. For the 935 nm wavelength laser the beam was tapped off from a beam dump which exists due to the losses in combining the laser beams sent to the ion trap with beam splitters. Further increases in the laser power sent to the cavities would require some of the power to be removed from the ion trap setup.

The reason for the method implemented to measure the linewidth was twofold, the frequency noise power spectral density provides a better characterisation of the laser frequency noise than the linewidth by itself and that the necessary equipment for other laser frequency noise characterisations were not available. No stable reference lasers were available for beatnote analysis of the laser frequency noise. A linewidth measurement using the delayed self heterodyne measurement as described in section 2.2 could not be performed due to a sufficiently long fiber not being available. The longest fiber available

was 20 m long, but using this would filter out the low frequency noise from technical sources, which was of interest for this project.

There was no independent method available to verify the accuracy of the linewidths obtained from the numerical integration of the frequency noise power spectral densities. The linewidth values presented in table 4.3 should be treated as lower bounds on the laser linewidths, since the same cavities were used for the measurements of the laser frequency noise as were used for stabilising the lasers. More accurate measurements of the laser linewidths can be performed using stable, high finesse cavities which are independent of the stabilization system.

4.3 Laser Frequency Stability

To determine the long term frequency drift of the lasers before and after stabilization the laser frequnecy was monitored using a wavelength meter as described in section. The temperature in the laboratory did not drift by more than 1° C during the measurement period as measure by a temperature logger placed on the optical table. The measurements were started at approximately the same time of day (16:00), as the laboratory temperature typically follows the outside ambient temperature. A post processing 1 minute average was applied to the data. The pre-and post stabilization frequency drifts measured over a 5 hour period for the 739 nm wavelength laser are shown in figure 4.9. The frequency drifts of the 935 nm wavelength laser pre- and post stabilization to the reference cavity are shown in figure 4.10.

The frequency drifts of the unlocked lasers are mainly caused by changes in the environmental conditions in the laboratory. The varying environmental conditions includes pressure, temperature and humidity. Electronic drifts in the laser driver current and temperature controllers may also play a role in the laser frequency drifts. These factors lead to the seemingly random behaviour of the free running laser frequencies observed in figures 4.9 and 4.10.

The drifts in the locked laser frequencies can be due to two factors, changes in the cavity resonance frequency and drift in the lockpoint of the feedback loop. Drifts in the lockpoint should be at most on the order of the cavity linewidth, as the linearity of the PDH error signal is only valid on these scales and the laser will not remain resonant with the cavity outside this lin-

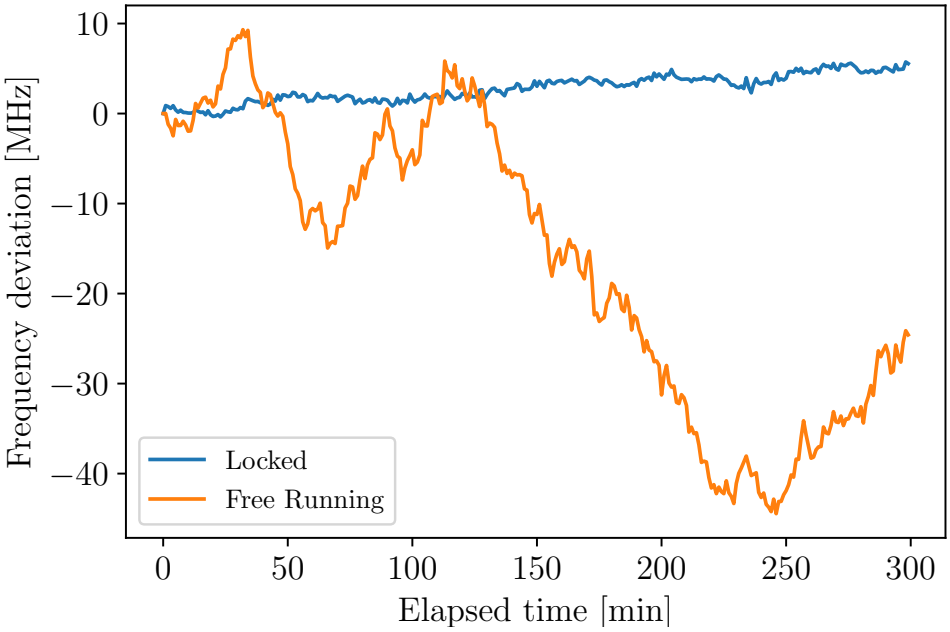

Figure 4.9: Laser frequency drift of 739 nm wavelength laser when free running and when locked to the reference cavity.

ear regime. Large frequency drifts must be due to cavity resonance frequency drifts due to changes in the cavity optical path length. The slow nature of the observed drifts in the locked laser frequency suggests that the cause is thermal drift of the cavity spacer length. The drift in the wavelength meter reading is unknown, but is assumed to be negligible for the measurement purposes. If desired, the drift of the wavelength meter can be determined by performing a spectroscopy experiment on a trapped ion with the lasers locked to the reference cavities, as trapped ions make excellent drift immune optical frequency references.

The locked 739 nm wavelength laser exhibits a linear drift of 1 MHz/h during the measurement period. The locked 935 nm wavelength laser had a non-monotonic 2.5 MHz up and 2.5 MHz down drift during the measurement period. The observed linear drifts in the locked 739 nm wavelength laser frequency can be equated to an average temperature change of 0.0025 °C per hour if only thermal expansion of the cavity spacer is considered. The two reference cavities are expected to expand by almost identical amounts, as the cavities are practically identical, but the 739 nm is expected to drift by a factor

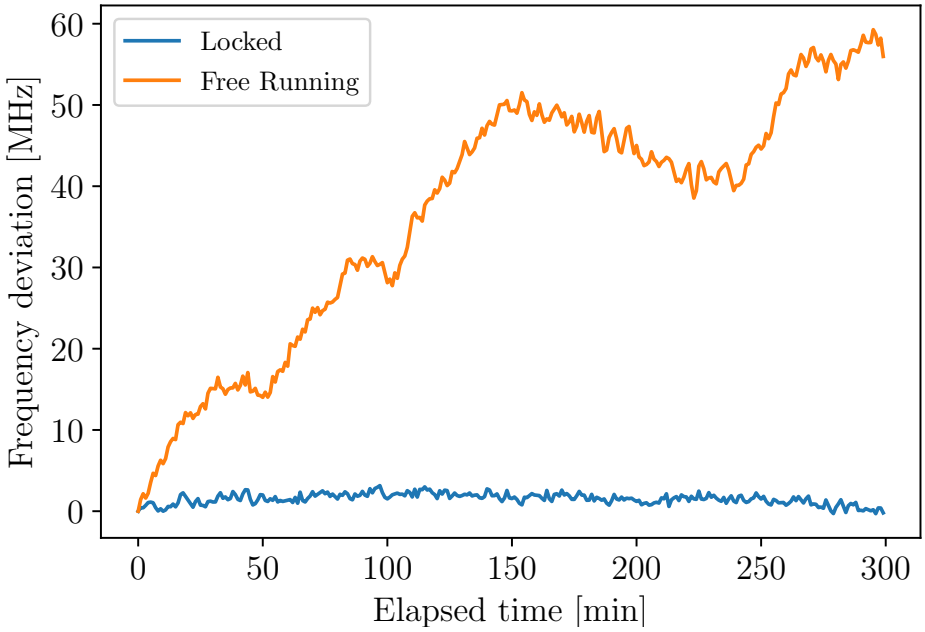

Figure 4.10: Laser frequency drift of 935 nm wavelength laser when free running and when locked to the reference cavity.

935/739 $\approx$ 1.3 more than the 935 nm for a given temperature change. This is calculated using equation 2.3.8. The 935 nm non-monotonic drift could be due to a slow oscillation in the temperature controller output.

Invar was chosen as the spacer material for the cavities, this was mainly to limit the cost of using ceramic spacers such as Zerodur or ULE, which have lower CTE values. The Invar could also be machined by the in-house workshop further cutting down on expenses. To achieve the desired sub MHz drifts over the few hour time span the pressure can fluctuate by no more than 0.01 mbar and the temperature of the cavity by no more than 0.0025 °C, as calculated using equitations 2.3.6 and 2.3.8. The vacuum chamber served to reduce the pressure fluctuations well below the desired limit as the absolute pressure was on the order of 5×10^{-7} mbar. The ambient laboratory temperature is typically stable to within 1 degree Celsius. The temperature control of the chamber should further improve on the thermal stability of the cavities. The rated linear stability of the temperature controller used was 0.0009 °C over 1 h and 0.002 °C over 24 h [48]. The cavities had no direct contact with the chamber walls, only with the PTFE mounts. The PTFE used has a thermal conductivity of

0.20 W/m.K [49] compared to 14.25 W/m.K [50] for 304L stainless steel. This should reduce the rate of thermal conduction between the cavities and vacuum chamber walls. The low pressure inside the vacuum chamber further aids in reducing thermal transfer between the cavities and the chamber walls due to reduced convection. No radiation shield had been placed in the chamber due to space limitations. A radiations shield would promote even heating of cavities and further lower thermal transfer between the cavities and the chamber walls. The excess temperature drift may be due to the temperature controller and heating pads being underpowered for the size of the vacuum chamber. A plot of the locked 739 nm frequency drift with the vacuum chamber surface temperature deviations is shown in figure 4.11. Figure 4.12 shows the 739 nm wavelength laser freqency drift with the laboratory temperature.

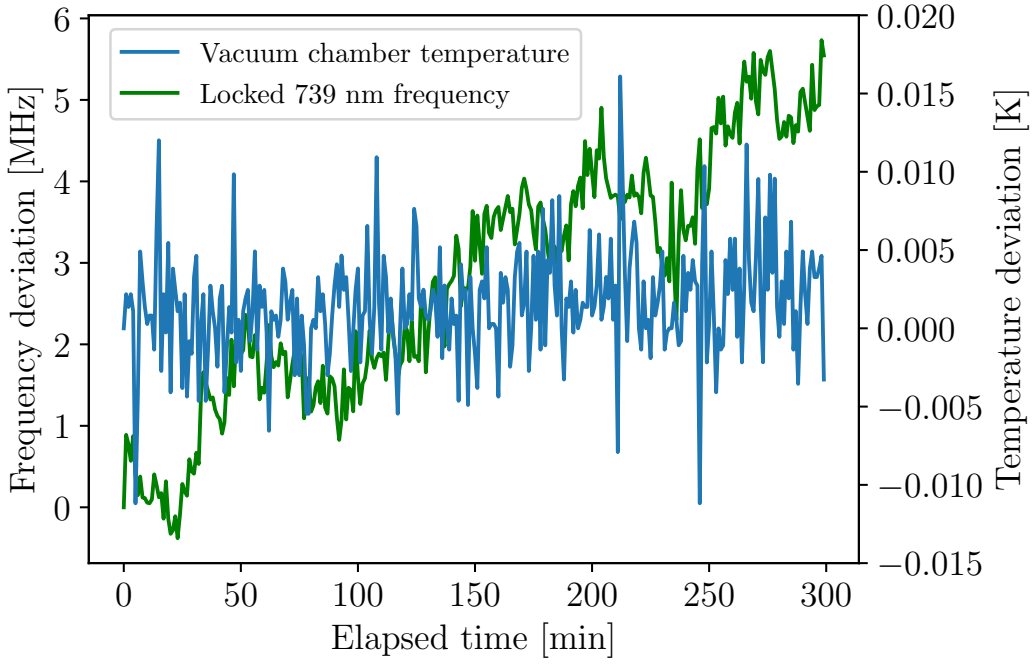

Figure 4.11: Laser frequency drift of the locked 739 nm wavelength laser with the vacuum chamber temperature deviation.

The laboratory temperature was measured with a temperature logger and the vacuum chamber surface temperature was measured by monitoring the voltage over the temperature controller's thermistor with a USB DAQ. The voltage was converted to temperate using the Steinhart-Hart equation with the coefficients of the thermistor provided by the manufacturer. From figures

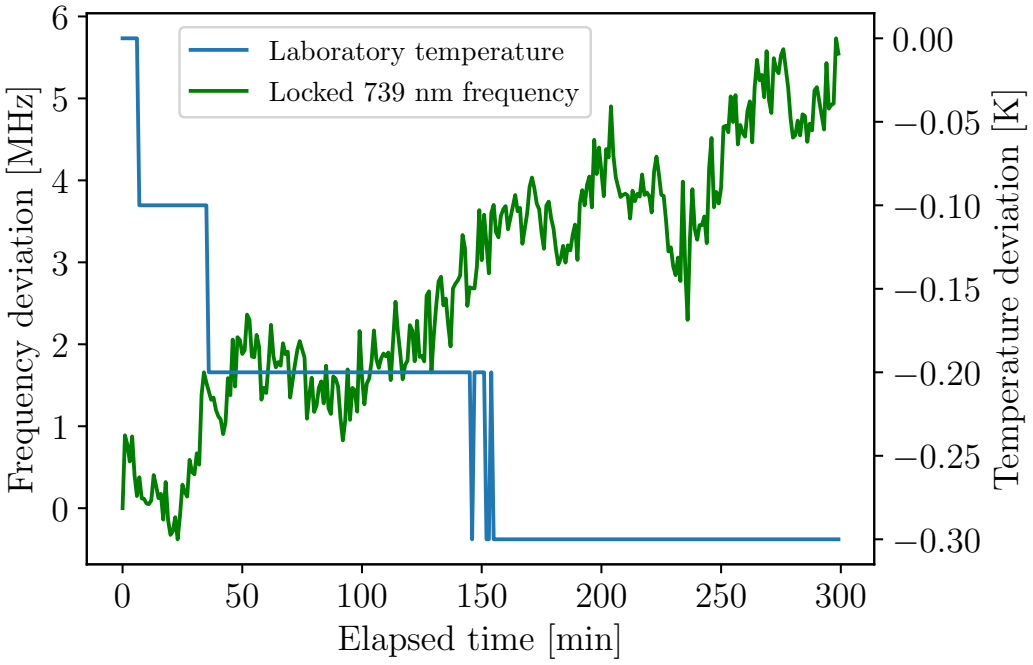

Figure 4.12: Laser frequency drift of the locked 739 nm wavelength laser with the laboratory temperature deviation.

4.11 and 4.12 the locked laser frequency drift appears to be correlated with the laboratory temperature. A similar correlation between the chamber temperate and the laser frequency was not observed. It should be noted that the thermistor samples the temperature at a singe location on the vacuum chamber surface. This means that the controller cannot respond the changes in the local temperature of the chamber at other locations. The standard deviation of the chamber temperature was 0.02 K during the measurement period. This temperature fluctuation measurement is influenced by the voltage noise of the USB DAQ, which is specified as 0.5 mVrms [51]. The standard deviation of the voltage used to deduce the chamber temperature was 0.6 mV. A linear fit to the chamber temperature shows a temperature drift of -0.0005 K/h.

The temporal dimensional stability of Invar is dependant on the heat treatment process, temperature, time since heat treatment and carbon content of the Invar sample [52]. The exact initial heat treatment and purity of the Invar used for this project was unknown. No heat treatment was performed after the machining of the cavities. All of the measurements reported in this thesis were performed at least six months after the machining of the cavities. Berthold *et al.* [53] measured the dimensional stability of an Invar cavity as $\Delta L/L =$

$(5.64 \pm 0.03) \times 10^{-9}$ per day. The Invar Berthold *et al.* [53] used was initially heat treated in a three step heating process and not treated again after machining. This temporal instability would lead to drifts of approximately 100 kHz/h in the laser frequency when locked to the reference cavity used in this project, provided that the Invar used had similar properties to that used by Berthold *et al.* [53]. This can be thought of as the upper limit to the long term stability of the cavities as this is independent of the quality of the temperature control or pressure stability.

4.4 Simultaneous Laser Frequency and Cavity Length Stabilization

To stabilize the laser to the cavity and to simultaneously stabilize the cavity free spectral range to a microwave frequency two error signals are required. The lock of the laser to the cavity (carrier lock) is performed using the signal which is generated by the 12.5 MHz demodulation. The cavity free spectral range lock (length lock) is performed using the 4 MHz demodulated signal. The details about the generation of these signals and locking electronics are described in section 3.5.

The change in the q'th cavity resonance frequency due to a cavity length change ΔL can be approximated as

$$\Delta\nu_q \approx \frac{\nu_q \Delta L}{L} = \frac{qc\Delta L}{2L^2}. \tag{4.4.1}$$

The tunable cavity was designed to be as short as possible, since the change in free spectral range for a change in cavity length scales with $1/L^2$. This gives a larger sensitivity to changes in cavity length by measuring the free spectral range for a shorter cavity. The cavity linewidth scales with $1/L$, hence the use of higher reflectivity mirrors for the tunable cavity than for the longer reference cavities. The trade-off in cavity linewidth can, however, be avoided by modulating at a larger integer multiple of the cavity free spectral range, since the slope of the cavity length error signal scales with the sideband frequency. This can be simply explained since the cavity length change is measured by observing the change in frequency of the m'th resonance frequency relative to the n'th resonance frequency, where the n'th resonance frequency is

the laser carrier frequency and $m = n + \Omega/(2\pi\nu_{FSR})$ where Ω is the sideband angular frequency and ν_{FSR} is the cavity free spectral range [2]. The alternative solution was realized after machining of the cavity spacer, and the final cavity construction therefore was made as long as was allowed for by the already constructed spacer to reduce the cavity linewidth. Another oversight was that the actual length of the cavity is not the quantity that must be stabilized, it is the n'th resonance frequency. The change in cavity resonance frequency due to a length change also scales with $1/L^2$, effectively removing the need for a shorter cavity entirely, provided that the cavities exhibit the same resonance frequency change due to environmental disturbances. Typically the vibrational sensitivity of optical cavities are length dependant. The thermal stability of the cavity resonance frequencies are length independent as shown in equation 2.3.8.

The reasoning for our choice of method to generate the free spectral range error signal was that to implement the method of Defoe and Brewer [39] on the cavity would require the photodetecor and demodulation electronics to function in the 4 GHz regime, whereas the method implemented in this project requires it to only function at 4 MHz. The implemented method differs from the method implemented by Belfi *et al.* [35] in that their modulation frequency for the sideband error signal was a frequency dithering whereas the modulation implemented in this project was in the PDH regime. The larger 4 MHz modulation frequency gives the steeper linear error signal slope of the PDH signal compared to the dithered signal. The methods also differ in that their method was used to lock the cavity length to a stabilized Helium-neon laser and the modulation sidebands were used to monitor the change in cavity length. In the method attempted in this project the laser was locked to the cavity and the cavity length was intended to be locked to the modulation sidebands which matches an integer multiple of the cavity free spectral range.

The 4 MHz demodulated cavity free spectral range error signal is shown in figure 4.13. The displayed signal is the average of three measurements. This signal has the desired linear slope with a zero crossing where the 4 GHz matches the cavity free spectral range [3]. The slope of the signal was determined by a

[2]For the original cavity design it was assumed that m - n = 1, which is not necessarily the case.

[3]There was a DC offset present on the oscilloscope which was not present on the lock in amplifiers digital display.

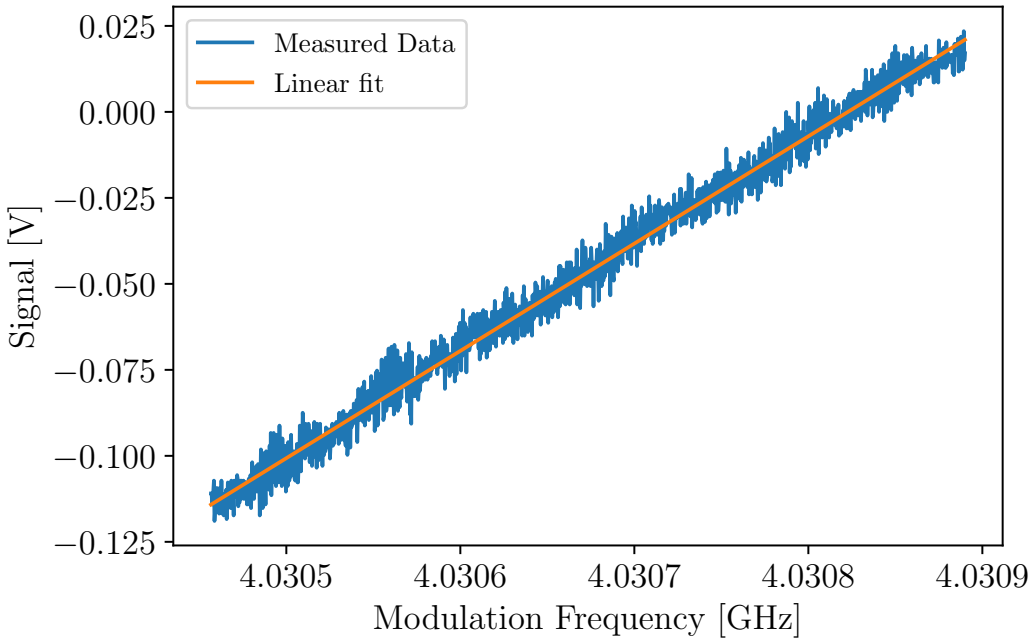

Figure 4.13: Free Spectral Range Error Signal

linear fit and this slope was 312 ± 4 mV/MHz [4]. For a change in free spectral range ΔF the q'th resonance frequency changes by an amount $\Delta\nu_q = \frac{2L\nu_q\Delta F}{c} = q\Delta F$. Adjusting the changes in free spectral range to changes in the resonance frequency to which the laser is locked to results in a slope of 7.844 μV/MHz. To achieve the desired lock a 7.844 μV change in voltage had to be detected. It was not possible to be detect the 7.844 μV voltage change due to the presence of voltage noise. The frequency spectrum of the error signal voltage noise was determined by removing the linear trend from the data and performing a FFT. The result of this is shown in figure 4.14. There are clear spikes at 50 Hz and 100 Hz in the frequency spectrum of the voltage noise corresponding to the 50 Hz frequency of the mains supply power. The stability of the carrier lock also has an influence on the noise of the free spectral range error signal. The slope of the free spectral range error signal and hence the performance of the cavity length lock can be improved by increasing the laser power sent to the cavity. This could not be done due to the optical feedback discussed in section 4.2. The laser power that could be sent to the cavity was limited to 0.155 mW in order to maintain a stable lock of the laser to the cavity. The

[4]Uncertainty specified as standard error of the slopes of the linear fits of the three measurements.

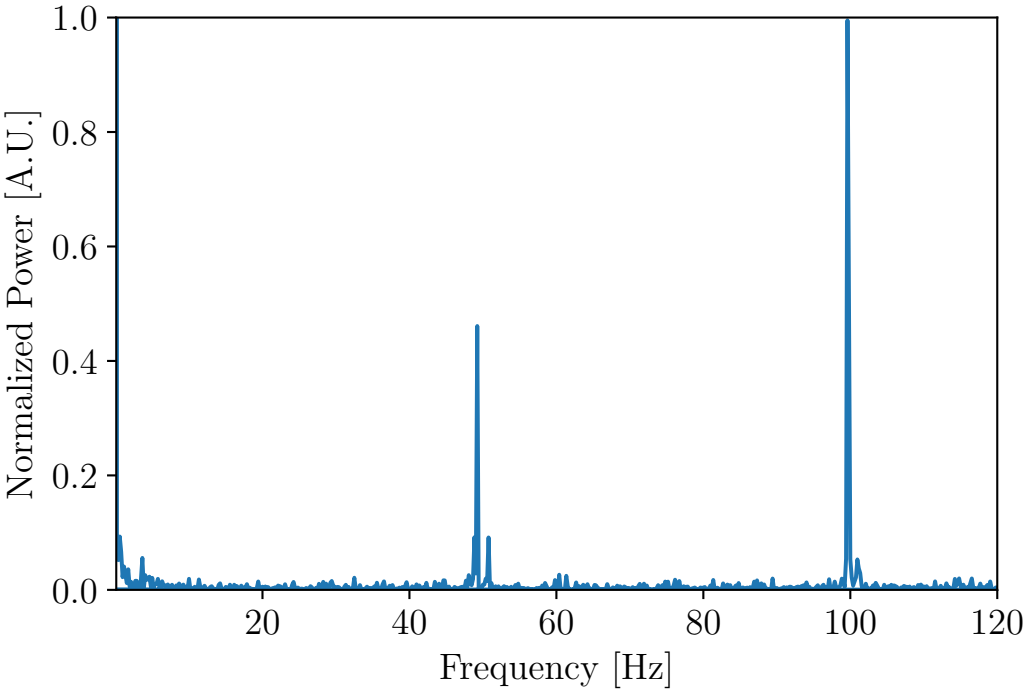

Figure 4.14: Frequency spectrum of the voltage noise of the cavity free spectral range error signal.

maximum power which can be sent to the cavity is 9 mW, as limited by the mode matching into the fiber EOM. The amplitude of the 4 GHz signal and hence the modulation depth was set at a trade off between carrier lock stability and free spectral range lock error signal magnitude. Increasing the laser power will also improve the carrier lock which will remove some of the noise from the length lock signal, since the length lock signal is dependant on the carrier detuning from cavity resonance. In an attempt to further limit back reflections the wave plates used between the fiber EOM and cavity were tilted slightly from normal incidence.

The design of a photodetector with built in amplifier, mixer, low pass filter and signal digitizer was commissioned to serve as the detector for this setup. This detector was ultimately not used due to the small sideband error signal requiring external amplification and the lock in amplifier provided lower noise in the demodulation path.

Chapter 5

Conclusion and Outlook

5.1 Conclusion

Two Pound-Drever-Hall laser frequency stabilization systems were designed and constructed with custom built optical reference cavities serving as the optical frequency references. These systems were used to stabilize the frequencies of a 935 nm wavelength external cavity diode laser and a 739 nm wavelength external cavity diode laser which acts as the seed laser for the second harmonic generation of a 369 nm laser for use in the Yb^+ linear Paul trap. The long term drifts of the laser frequencies had been shown to follow the drifts of the cavity resonance frequencies. The laser frequency drifts are 1 MHz/h as measured over a 5 hour period. The drifts in the cavity resonance frequencies had been established to be due to temperature changes. The post-stabilization drifts had been shown to reduce the random behaviour of the free running laser frequencies. The laser frequency noise power spectral densities have been determined by measuring the voltage noise power spectral densities of PDH error signals with the reference cavities acting as the frequency references. A reduction in the low frequency noise of the laser frequencies has been established for the locked lasers when compared to the free running lasers. The linewidths of the lasers for various integration times have been estimated from the frequency noise power spectral densities. These estimates are lower bounds on the laser linewidths, as the cavities used were not independent of the stabilization system. An additional piezoelectrically tunable cavity was also designed and constructed. A dual PDH technique was implemented to attempt to stabilize the free spectral range and hence length of the cavity to

a microwave frequency referenced to a Rubidium frequency standard whilst the laser was locked to the cavity. The method did not work due to the small slope of the cavity length lock error signal. The small slope resulted in the inability to detect cavity length changes on the scale of interest. The limiting factor of the slope of the error signal is due to the necessary limiting of the optical power incident on the cavity due to optical feedback from the cavity reflections destabilising the laser frequency. The insertion of an optical isolator in the beam line will eliminate the optical feedback and allow for increased laser power sent to the cavity.

5.2 Outlook

Currently the cavity resonances are not resonant with the desired ion transitions. The portion of the laser beam sent to the cavities must be frequency shifted to match a cavity resonance whilst the main laser output is resonant with the ion transitions. An EOM can be used to produce sidebands for an offset sideband lock or an AOM can be used to produce the desired frequency shift. The power of the shifted beam incident on the cavity must be considered to maximize the slope of the PDH error signal. The stability of the RF source used to produce the shift will influence the stability of the laser frequency. The tunability of the RF used to produce the shift will depend on the trapped ion experiments which will be performed. The minimum requirement of the tuning of the RF is that the frequency must be able to be tuned over at least half a cavity free spectral range, as this will allow the laser to always be within tuning distance from a cavity resonance. The planned implementation for the 935 nm is to use a signal generated with a direct digital synthesizer which is referenced to a Rubidium frequency standard to generate the tunable RF signal which will be applied to the fiber EOM in addition to the 3 GHz already applied for the required sidebands for the trapped ion experiments. These signals will be combined using a Mini-Circuits ZFRSC-42-S+ RF power combiner with the combined signal sent to the fiber EOM. For the 739 nm wavelength laser a Qubig EO-T1190M3-VIS resonant EOM is available to produce the sidebands for an offset sideband lock, but due to the resonant design of the EOM tunability is limited. The EOM has a resonance bandwidth of 3.1 MHz and the resonance can be tuned over the range 959 - 1314 MHz via a tuning

screw. The longevity of the device with frequent tuning via the tuning screw is in doubt. To avoid potential damage to the resonant EOM it has not been used for an offset sideband lock. For greater tunability a non resonant EOM or a tunable AOM will be required. An Analog Devices ADF4350 phase locked loop frequency synthesizer evaluation board and a Mini-Circuits TVA-11-422 amplifier have been shown to be able to produce sidebands with the resonant EOM.

Further improvements on the temperature stabilization of the cavities can be made to improve the frequency drift performance of the lasers. It is also possible to change the frequency of the RF used to produce the frequency shift to cavity resonance to remove the drifts which are observed using the wavelength meter. Measurements of the laser linewidths via the delayed self heterodyne method or frequency noise power spectral densities measured over larger frequency ranges with more stable optical frequency references might be desired depending on the experiments planned to be performed using the ion trap. For convenience the turbomolecular pump should be exchanged for an ion pump. An additional optical isolator might be required to improve the frequency noise performance of the 935 nm wavelength laser.

Appendices

Appendix A

Technical Drawings

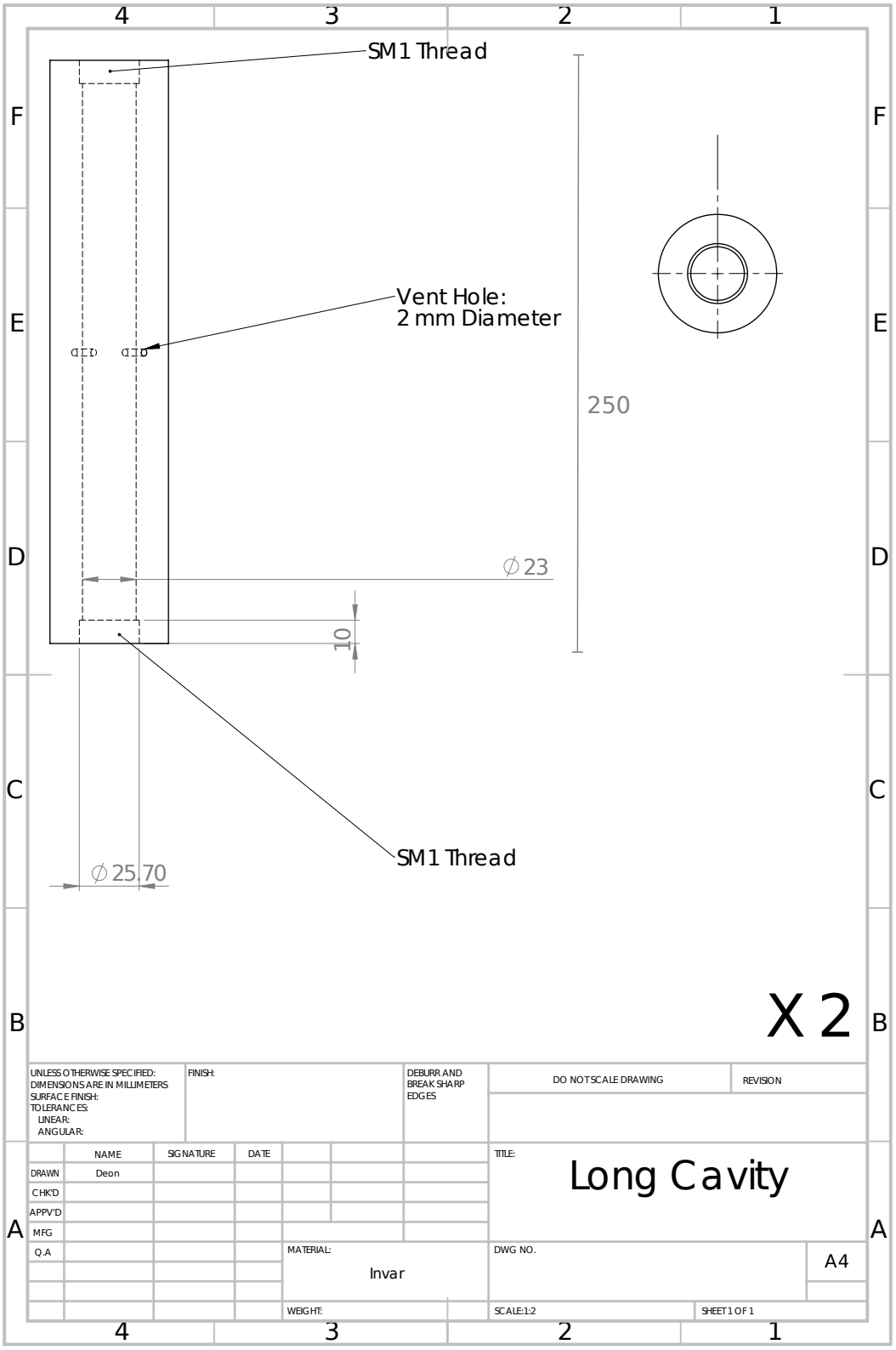

Figure A.1: Drawing of Invar spacer for 23 cm reference cavities.

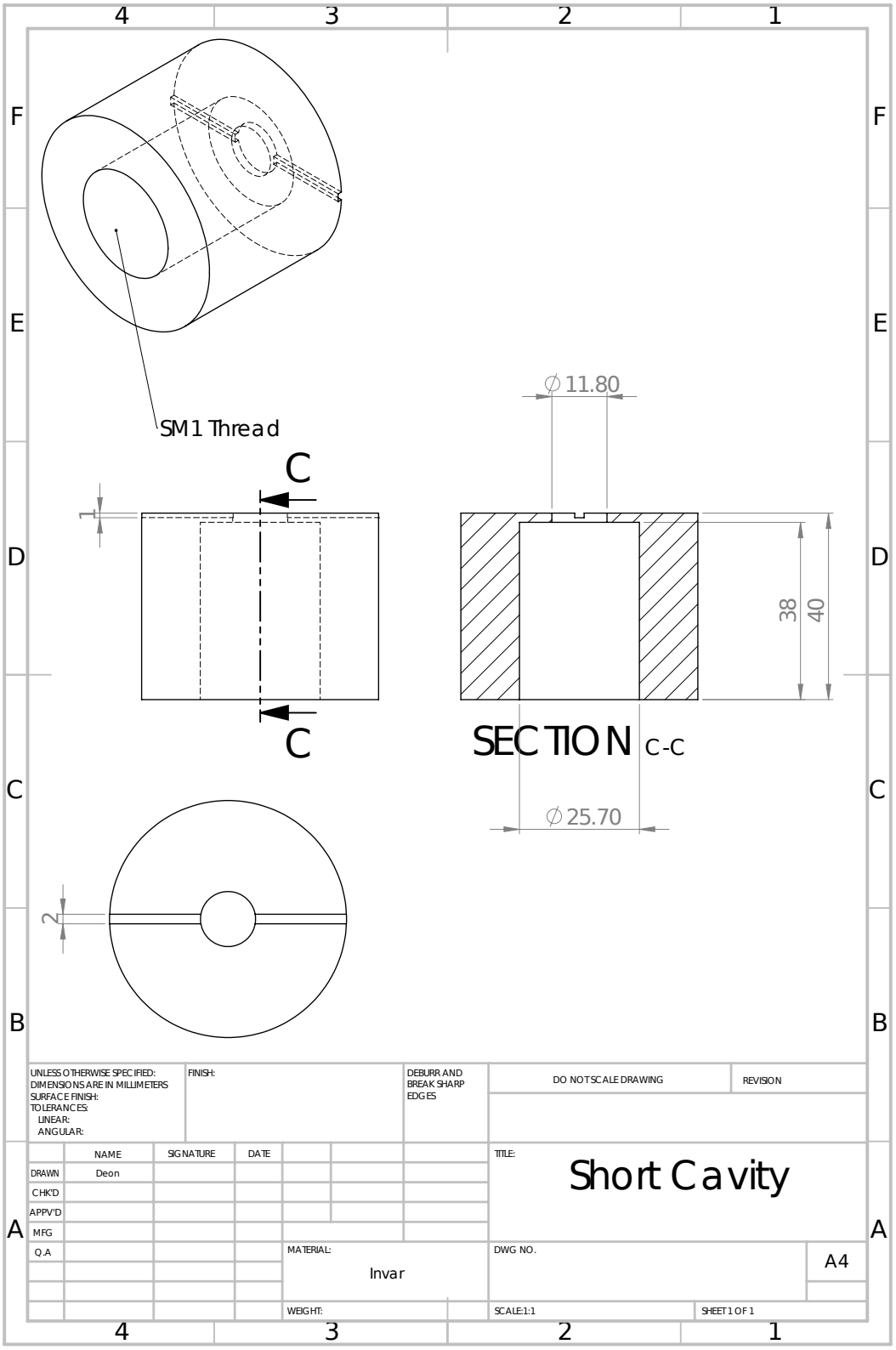

Figure A.2: Drawing of Invar spacer for tunable cavity

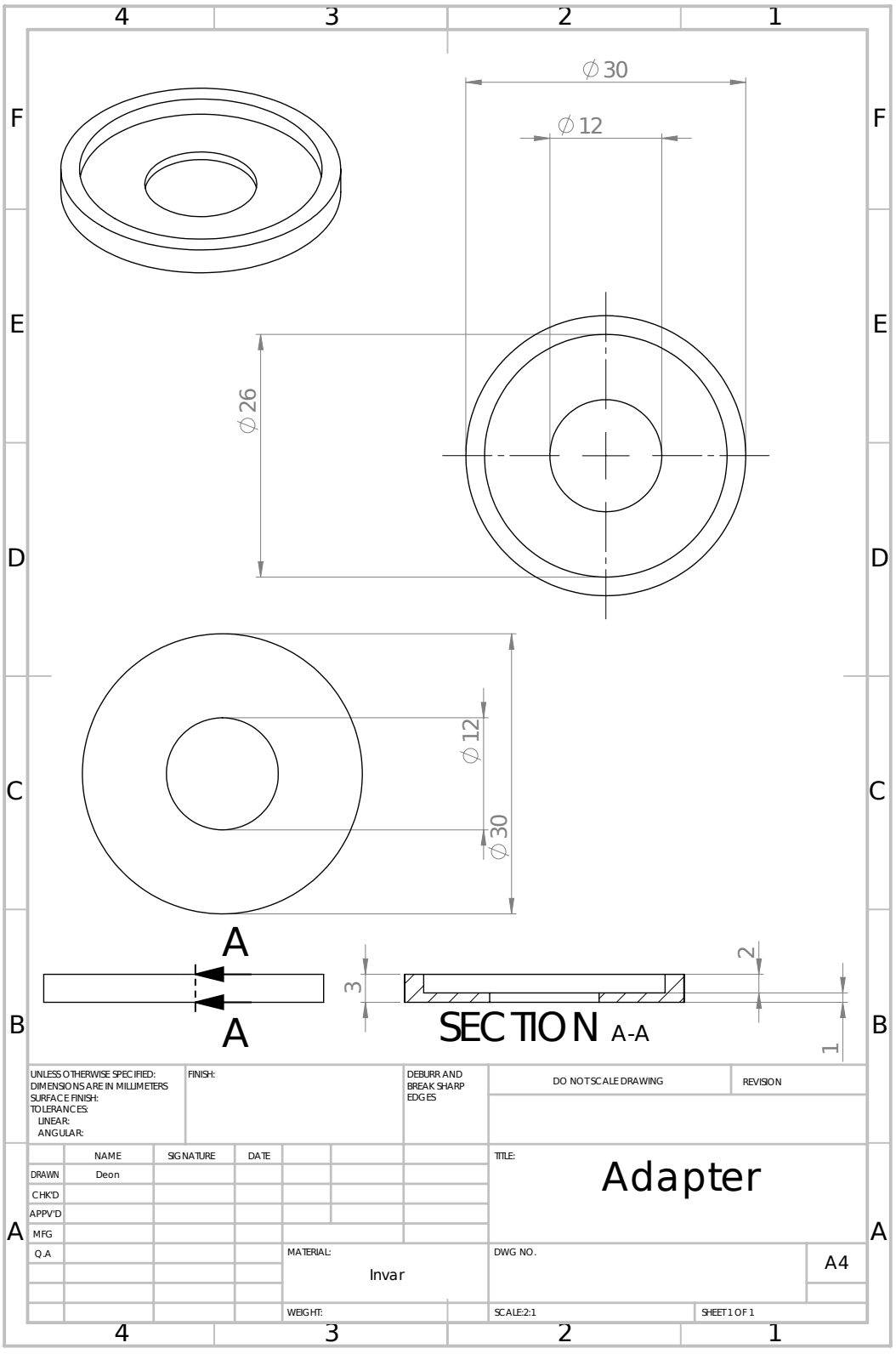

Figure A.3: Drawing of Invar adapter for gluing mirror to piezo for the tunable cavity

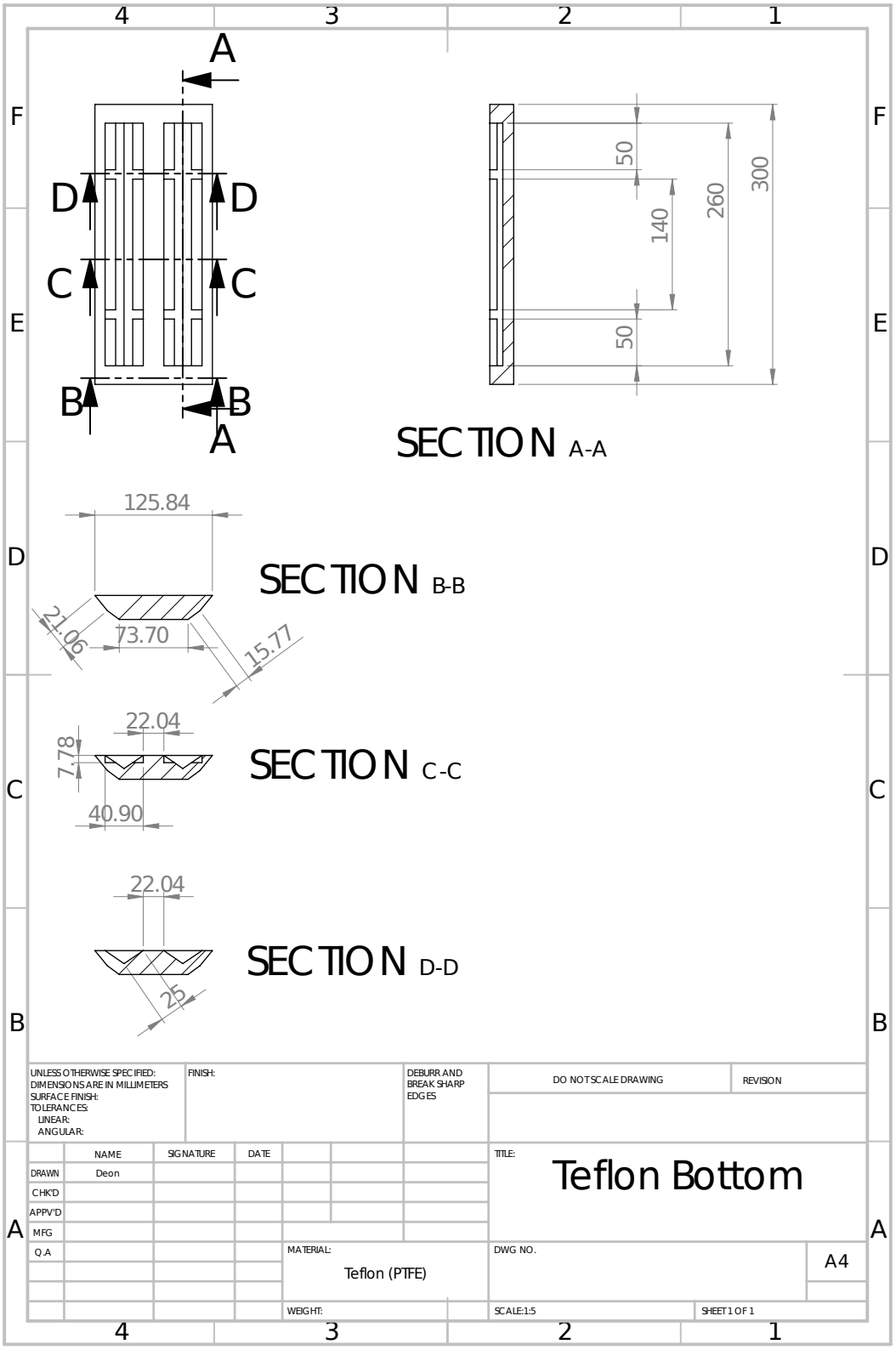

Figure A.4: Drawing of PTFE bottom mount for cavities in vacuum chamber

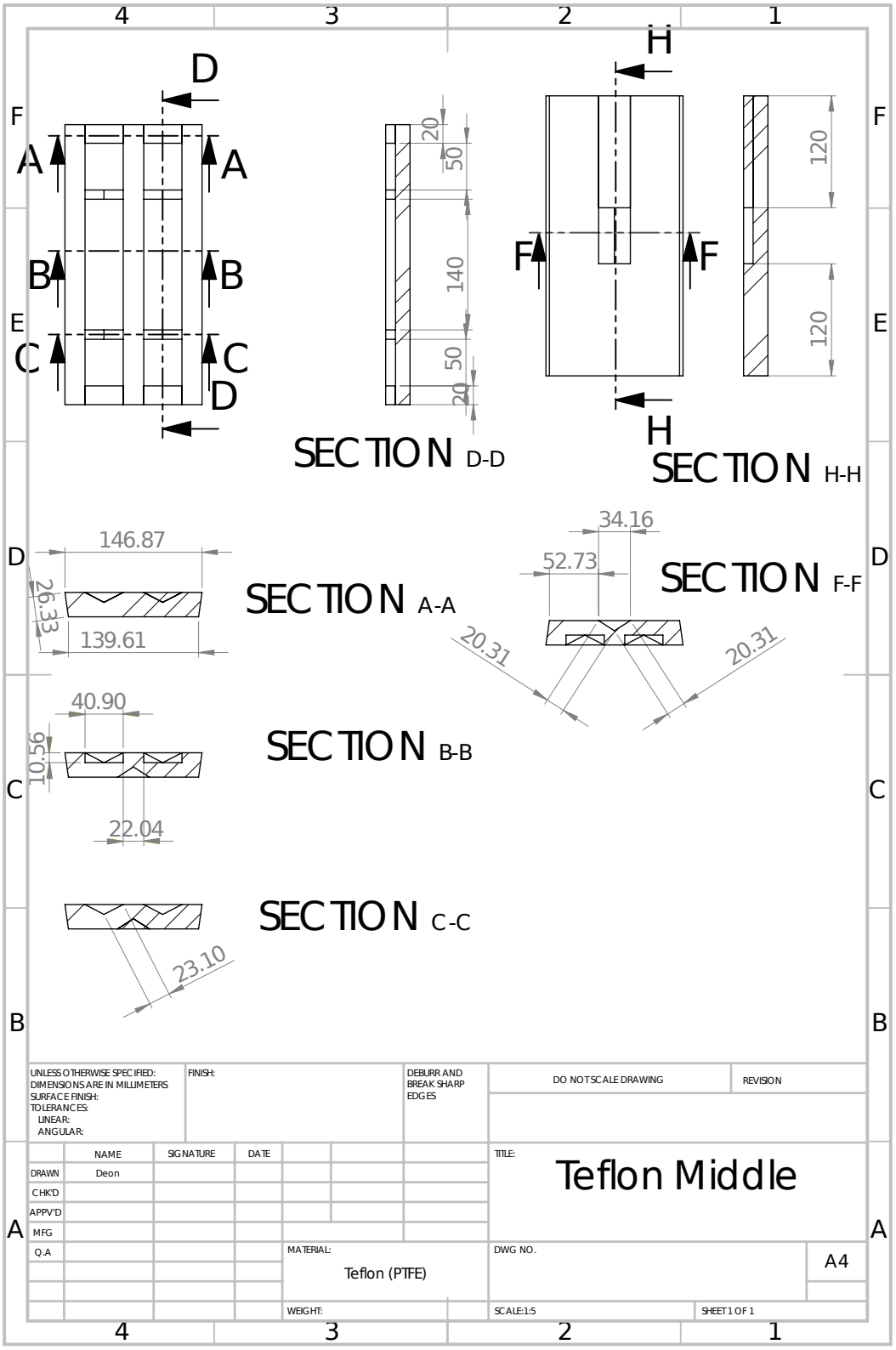

Figure A.5: Drawing of PTFE upper mount for cavities in vacuum chamber

Appendix B

Derivation and Numerical Investigation of Free Spectral Range Lock Error Signal

This chapter derives and investigates the error signals for locking a laser to a cavity and locking the cavity free spectral range to an RF signal simultaneously.

B.1 Derivation

Consider a cavity of length L, free spectral range $\nu_{FSR} = \frac{c}{2L}$ and mirror reflection coefficient r. The reflection transfer function of the cavity as a function of angular frequency is given by the expression

$$R(\omega) = \frac{r(e^{i\frac{\omega}{\nu_{FSR}}} - 1)}{1 - r^2 e^{i\frac{\omega}{\nu_{FSR}}}}. \tag{B.1.1}$$

Let the light incident on the cavity have angular frequency ω and amplitude E_0. To produce a PDH lock of the laser to the cavity the laser is phase modulated with modulation index a at angular frequency α. To produce the sidebands close to ν_{FSR} an additional phase modulation with modulation index b at angular frequency β. The value of β is single tone frequency modulated with the modulation signal $\Delta f \cos(\gamma t)$ where γ is the modulation angular frequency and Δf is the frequency deviation. This gives the modulation index $c = \frac{2\pi\Delta f}{\gamma}$.

This produces the light incident on the cavity

$$E_i(t) \quad = \quad E_0 e^{i\omega t + ia\sin(\alpha t) + ib\sin(\beta t + c\sin(\gamma t))}. \tag{B.1.2}$$

Assuming that for all the modulations the modulation indices are small enough that the power is situated exclusively in their carriers and first order sidebands then the incident electric field can simplify as follows:

$$\begin{aligned}
E_i(t) &\approx E_0 e^{i\omega t}\left(J_0(a) + J_1(a)e^{i\alpha t} - J_1(a)e^{-i\alpha t}\right) e^{ib\sin(\beta t + c\sin(\gamma t))} && [a<1] \\
&\approx E_0 e^{i\omega t}\Big(J_0(a) + J_1(a)e^{i\alpha t} - J_1(a)e^{-i\alpha t}\Big)\Big(J_0(b) + J_1(b)e^{i(\beta t + c\sin(\gamma t))} \\
&\quad - J_1(b)e^{-i(\beta t + c\sin(\gamma t))}\Big) && [b<1] \\
&\approx E_0 e^{i\omega t}\Big(J_0(a) + J_1(a)e^{i\alpha t} - J_1(a)e^{-i\alpha t}\Big)\Big(J_0(b) + J_1(b)e^{i\beta t}\Big(J_0(c) \\
&\quad + J_1(c)e^{i\gamma t} - J_1(c)e^{-i\gamma t}\Big) - J_1(b)e^{-i\beta t}\Big(J_0(c) + J_1(c)e^{-i\gamma t} - J_1(c)e^{i\gamma t}\Big)\Big) \\
& && [c<1] \\
&= E_0\Big(J_0(a)e^{i\omega t} + J_1(a)e^{i(\omega+\alpha)t} - J_1(a)e^{i(\omega-\alpha)t}\Big)\Big(J_0(b) + J_1(b)J_0(c)e^{i\beta t} \\
&\quad + J_1(b)J_1(c)e^{i(\beta+\gamma)t} - J_1(b)J_1(c)e^{i(\beta-\gamma)t} \\
&\quad - J_1(b)J_0(c)e^{-i\beta t} - J_1(b)J_1(c)e^{-i(\beta+\gamma)t} + J_1(b)J_1(c)e^{-i(\beta-\gamma)t}\Big)
\end{aligned}$$

$$\begin{aligned}
&= E_0\Big(J_0(a)J_0(b)e^{i\omega t} + J_0(a)J_1(b)J_0(c)e^{i(\omega+\beta)t} - J_0(a)J_1(b)J_0(c)e^{i(\omega-\beta)t} \\
&\quad + J_0(a)J_1(b)J_1(c)e^{i(\omega+\beta+\gamma)t} - J_0(a)J_1(b)J_1(c)e^{i(\omega+\beta-\gamma)t} \\
&\quad - J_0(a)J_1(b)J_1(c)e^{i(\omega-\beta-\gamma)t} + J_0(a)J_1(b)J_1(c)e^{i(\omega-\beta+\gamma)t} \\
&\quad + J_1(a)J_0(b)e^{i(\omega+\alpha)t} + J_1(a)J_1(b)J_0(c)e^{i(\omega+\beta+\alpha)t} \\
&\quad - J_1(a)J_1(b)J_0(c)e^{i(\omega-\beta+\alpha)t} + J_1(a)J_1(b)J_1(c)e^{i(\omega+\beta+\gamma+\alpha)t} \\
&\quad - J_1(a)J_1(b)J_1(c)e^{i(\omega+\beta-\gamma+\alpha)t} - J_1(a)J_1(b)J_1(c)e^{i(\omega-\beta-\gamma+\alpha)t} \\
&\quad + J_1(a)J_1(b)J_1(c)e^{i(\omega-\beta+\gamma+\alpha)t} - J_1(a)J_0(b)e^{i(\omega-\alpha)t} \\
&\quad - J_1(a)J_1(b)J_0(c)e^{i(\omega+\beta-\alpha)t} + J_1(a)J_1(b)J_0(c)e^{i(\omega-\beta-\alpha)t} \\
&\quad - J_1(a)J_1(b)J_1(c)e^{i(\omega+\beta+\gamma-\alpha)t} + J_1(a)J_1(b)J_1(c)e^{i(\omega+\beta-\gamma-\alpha)t} \\
&\quad + J_1(a)J_1(b)J_1(c)e^{i(\omega-\beta-\gamma-\alpha)t} - J_1(a)J_1(b)J_1(c)e^{i(\omega-\beta+\gamma-\alpha)t}\Big)
\end{aligned} \tag{B.1.3}$$

The aforementioned approximations yields the reflected field

$$\begin{aligned}
E_r(t) = E_0\Big(& J_0(a)J_0(b)R(\omega)e^{i\omega t} + J_0(a)J_1(b)J_0(c)R(\omega+\beta)e^{i(\omega+\beta)t} \\
& - J_0(a)J_1(b)J_0(c)R(\omega-\beta)e^{i(\omega-\beta)t} \\
& + J_0(a)J_1(b)J_1(c)R(\omega+\beta+\gamma)e^{i(\omega+\beta+\gamma)t} \\
& - J_0(a)J_1(b)J_1(c)R(\omega+\beta-\gamma)e^{i(\omega+\beta-\gamma)t} \\
& - J_0(a)J_1(b)J_1(c)R(\omega-\beta-\gamma)e^{i(\omega-\beta-\gamma)t} \\
& + J_0(a)J_1(b)J_1(c)R(\omega-\beta+\gamma)e^{i(\omega-\beta+\gamma)t} \\
& + J_1(a)J_0(b)R(\omega+\alpha)e^{i(\omega+\alpha)t} + J_1(a)J_1(b)J_0(c)R(\omega+\beta+\alpha)e^{i(\omega+\beta+\alpha)t} \\
& - J_1(a)J_1(b)J_0(c)R(\omega-\beta+\alpha)e^{i(\omega-\beta+\alpha)t} \\
& + J_1(a)J_1(b)J_1(c)R(\omega+\beta+\gamma+\alpha)e^{i(\omega+\beta+\gamma+\alpha)t} \\
& - J_1(a)J_1(b)J_1(c)R(\omega+\beta-\gamma+\alpha)e^{i(\omega+\beta-\gamma+\alpha)t} \\
& - J_1(a)J_1(b)J_1(c)R(\omega-\beta-\gamma+\alpha)e^{i(\omega-\beta-\gamma+\alpha)t} \\
& + J_1(a)J_1(b)J_1(c)R(\omega-\beta+\gamma+\alpha)e^{i(\omega-\beta+\gamma+\alpha)t} \\
& - J_1(a)J_0(b)R(\omega-\alpha)e^{i(\omega-\alpha)t} - J_1(a)J_1(b)J_0(c)R(\omega+\beta-\alpha)e^{i(\omega+\beta-\alpha)t} \\
& + J_1(a)J_1(b)J_0(c)R(\omega-\alpha-\beta)e^{i(\omega-\beta-\alpha)t} \\
& - J_1(a)J_1(b)J_1(c)R(\omega-\alpha+\beta+\gamma)e^{i(\omega+\beta+\gamma-\alpha)t} \\
& + J_1(a)J_1(b)J_1(c)R(\omega-\alpha+\beta-\gamma)e^{i(\omega+\beta-\gamma-\alpha)t} \\
& + J_1(a)J_1(b)J_1(c)R(\omega-\alpha-\beta-\gamma)e^{i(\omega-\beta-\gamma-\alpha)t} \\
& - J_1(a)J_1(b)J_1(c)R(\omega-\alpha-\beta+\gamma)e^{i(\omega-\beta+\gamma-\alpha)t}\Big)
\end{aligned} \tag{B.1.4}$$

The photodetector detects the reflected power which is given by the expression $P_r(t) = |E_r(t)|^2$. Due to demodulation, for the PDH lock only the α and $-\alpha$ Fourier components are of interest and for the FSR lock only the γ and $-\gamma$ Fourier components are of interest. Define the quantities $P_{PDH}(t)$ and $P_{FSR}(t)$ which are the power terms of interest for the different demodulation

paths, where

$$
\begin{aligned}
P_{PDH}(t) = |E_0|^2 J_0(a) J_1(a) \Big(& e^{i\alpha t} \Big(J_0(b)^2 \Big(R(\omega+\alpha) R^*(\omega) \Big) \\
& + J_1(b)^2 J_0(c)^2 \Big(R(\omega+\beta+\alpha) R^*(\omega+\beta) + R(\omega-\beta+\alpha) R^*(\omega-\beta) \Big) \\
& + J_1(b)^2 J_1(c)^2 \Big(R(\omega+\beta+\gamma+\alpha) R^*(\omega+\beta+\gamma) \\
& + R(\omega+\beta-\gamma+\alpha) R^*(\omega+\beta-\gamma) + R(\omega-\beta-\gamma+\alpha) R^*(\omega-\beta-\gamma) \\
& + R(\omega-\beta+\gamma+\alpha) R^*(\omega-\beta+\gamma) \Big) \\
& - e^{-i\alpha t} \Big(J_0(b)^2 \Big(R(\omega-\alpha) R^*(\omega) \Big) \\
& + J_1(b)^2 J_0(c)^2 \Big(R(\omega+\beta-\alpha) R^*(\omega+\beta) + R(\omega-\beta-\alpha) R^*(\omega-\beta) \Big) \\
& + J_1(b)^2 J_1(c)^2 \Big(R(\omega+\beta+\gamma-\alpha) R^*(\omega+\beta+\gamma) \\
& + R(\omega+\beta-\gamma-\alpha) R^*(\omega+\beta-\gamma) + R(\omega-\beta-\gamma-\alpha) R^*(\omega-\beta-\gamma) \\
& + R(\omega-\beta+\gamma-\alpha) R^*(\omega-\beta+\gamma) \Big) \Big) \Big) \\
& + C.C.
\end{aligned}
\tag{B.1.5}
$$

and

$$
\begin{aligned}
P_{FSR}(t) = |E_0|^2 J_1(b)^2 J_1(c) J_0(c) \Big(& e^{i\gamma t} \Big(J_0(a)^2 \Big(R(\omega+\beta+\gamma) R^*(\omega+\beta) \\
& - R(\omega-\beta+\gamma) R^*(\omega-\beta) \Big) + J_1(a)^2 \Big(\\
& R(\omega+\beta+\gamma+\alpha) R^*(\omega+\beta+\alpha) - R(\omega-\beta+\gamma+\alpha) R^*(\omega-\beta+\alpha) \\
& + R(\omega+\beta+\gamma-\alpha) R^*(\omega+\beta-\alpha) - R(\omega-\beta+\gamma-\alpha) R^*(\omega-\beta-\alpha) \Big) \\
& + e^{-i\gamma t} \Big(J_0(a)^2 \Big(R(\omega-\beta-\gamma) R^*(\omega-\beta) \\
& - R(\omega+\beta-\gamma) R^*(\omega+\beta) \Big) + J_1(a)^2 \Big(\\
& R(\omega-\beta-\gamma+\alpha) R^*(\omega-\beta+\alpha) - R(\omega+\beta+\alpha-\gamma) R^*(\omega+\beta+\alpha) \\
& + R(\omega-\beta-\gamma-\alpha) R^*(\omega-\beta-\alpha) - R(\omega+\beta-\gamma-\alpha) R^*(\omega+\beta-\alpha) \Big) \Big) \Big) \\
& + C.C.
\end{aligned}
\tag{B.1.6}
$$

C.C has been used as shorthand to indicate the complex conjugate of the expression which precedes it.

Note that both $P_{PDH}(t)$ and $P_{FSR}(t)$ have the form

$$\begin{aligned} P(t) &= e^{i\nu t}g(x) + e^{-i\nu t}g^*(x) \\ &= \cos(\nu t)(g(x) + g^*(x)) + i\sin(\nu t)(g(x) - g^*(x)) \\ &= 2\cos(\nu t)\,\mathrm{Re}\{g(x)\} - 2\sin(\nu t)\,\mathrm{Im}\{g(x)\} \end{aligned} \tag{B.1.7}$$

for some complex function of frequency $g(x)$ and demodulation angular frequency ν. After demodulating with $\cos(\nu t + \phi)$ and low-pass filtering, a frequency dependant voltage $V(x) \propto \mathrm{Re}\{g(x)\}\cos(\phi) - \mathrm{Im}\{g(x)\}\sin(\phi)$ is produced. The error signals are

$$\begin{aligned} \epsilon_{PDH} = |E_0|^2 J_0(a)J_1(a)\ \mathrm{Im}\Big(\Big(&J_0(b)^2\Big(R(\omega+\alpha)R^*(\omega) - R^*(\omega-\alpha)R(\omega)\Big) \\ &+ J_1(b)^2J_0(c)^2\Big(R(\omega+\beta+\alpha)R^*(\omega+\beta) + R(\omega-\beta+\alpha)R^*(\omega-\beta) \\ &- R^*(\omega+\beta-\alpha)R(\omega+\beta) - R^*(\omega-\beta-\alpha)R(\omega-\beta)\Big) \\ &+ J_1(b)^2J_1(c)^2\Big(R(\omega+\beta+\gamma+\alpha)R^*(\omega+\beta+\gamma) \\ &+ R(\omega+\beta-\gamma+\alpha)R^*(\omega+\beta-\gamma) + R(\omega-\beta-\gamma+\alpha)R^*(\omega-\beta-\gamma) \\ &+ R(\omega-\beta+\gamma+\alpha)R^*(\omega-\beta+\gamma) - R^*(\omega+\beta+\gamma-\alpha)R(\omega+\beta+\gamma) \\ &- R^*(\omega+\beta-\gamma-\alpha)R(\omega+\beta-\gamma) - R^*(\omega-\beta-\gamma-\alpha)R(\omega-\beta-\gamma) \\ &- R^*(\omega-\beta+\gamma-\alpha)R(\omega-\beta+\gamma)\Big)\Big) \end{aligned} \tag{B.1.8}$$

$$\begin{aligned} \epsilon_{FSR} = |E_0|^2 J_1(b)^2J_1(c)J_0(c)\ \mathrm{Im}\Big(\Big(&J_0(a)^2\Big(R(\omega+\beta+\gamma)R^*(\omega+\beta) \\ &- R(\omega-\beta+\gamma)R^*(\omega-\beta) - R^*(\omega+\beta-\gamma)R(\omega+\beta) + R^*(\omega-\beta-\gamma)R(\omega-\beta)\Big) \\ &+ J_1(a)^2\Big(R(\omega+\beta+\gamma+\alpha)R^*(\omega+\beta+\alpha) - R(\omega-\beta+\gamma+\alpha)R^*(\omega-\beta+\alpha) \\ &+ R(\omega+\beta+\gamma-\alpha)R^*(\omega+\beta-\alpha) - R(\omega-\beta+\gamma-\alpha)R^*(\omega-\beta-\alpha) \\ &+ R^*(\omega-\beta-\gamma+\alpha)R(\omega-\beta+\alpha) - R^*(\omega+\beta+\alpha-\gamma)R(\omega+\beta+\alpha) \\ &+ R^*(\omega-\beta-\gamma-\alpha)R(\omega-\beta-\alpha) - R^*(\omega+\beta-\gamma-\alpha)R(\omega+\beta-\alpha)\Big)\Big) \end{aligned} \tag{B.1.9}$$

B.2 Numerical Investigation

The simulation parameters used were the same as for the experimental setup described in section 3.5. These parameters are summarised in table B.1.

Table B.1: Simulation parameters

Quantity	**Value**
Mirror Reflectance	0.999
Laser Wavelength	935 nm
Cavity Length	37 mm
α	12.5 MHz
a	1.08
γ	4 MHz
c	1.08

It should be noted that for the carrier lock the maximum slope is achieved with $a = 1.08$ and for the FSR lock the maximum slope is achieved with $c = 1.08$. This is consistent with the normal PDH error signal, as the maximum of $J_0(a)J_1(a)$ is achieved with $a = 1.08$ [34]. Close to resonance the error signal for the lock of the carrier is the regular PDH signal. The signal slope is dependant on the modulation depth of the β frequency. This is shown in figure B.1 and the dependence is due to the reduced power in the carrier and α sidebands for increased b. The slope of the signal is also dependant on the

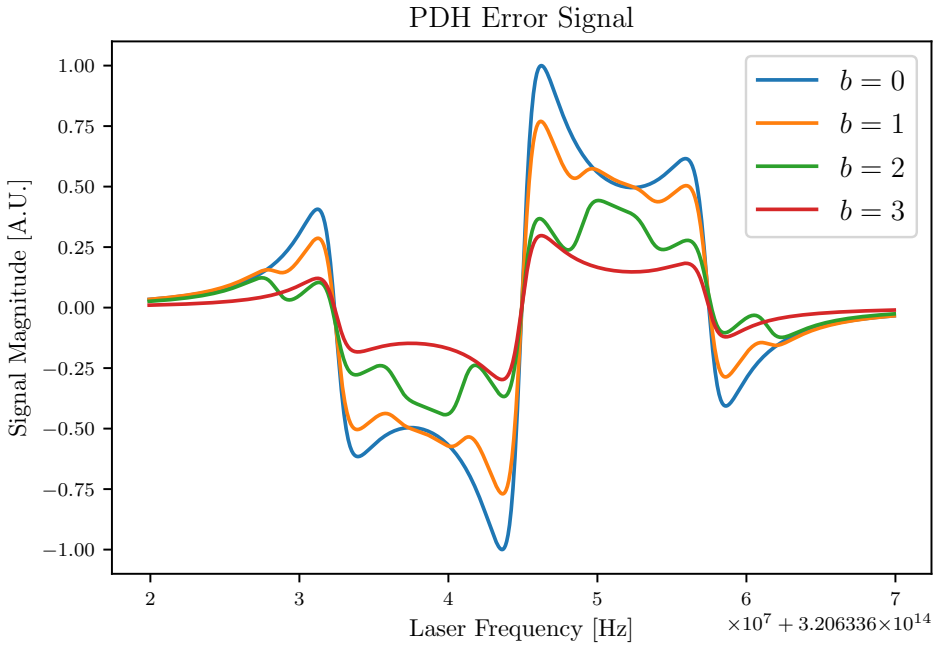

Figure B.1: Simulated PDH carrier lock error signal.

detuning of $\frac{\beta}{2\pi}$ from the cavity free spectral range as shown in figure B.2. The

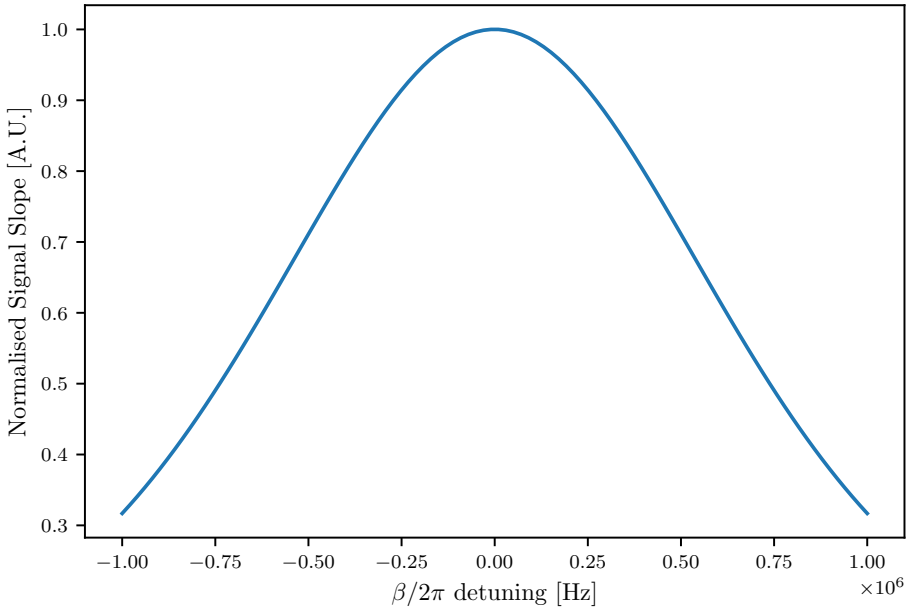

Figure B.2: Simulated PDH carrier lock error signal slope with β detuning.

b dependence of the FSR lock slope is due to the $J_1(b)^2$ factor, which has a maximum at $b = 1.84$. It should be noted that the PDH error signal slope also has a $J_0(b)^2$ dependence. This results in a trade-off between PDH and FSR error signal slope. The maximum value of $J_1(b)^2$ corresponds to a slope of the PDH signal which is a tenth of its maximum value. The FSR error signal has the desired zero crossing when $\frac{\beta}{2\pi}$ matches the cavity free spectral range and linear slope close to resonance as shown in figure B.3. . The FSR signal slope is also dependant on the carrier detuning from resonance as shown in figure B.4.

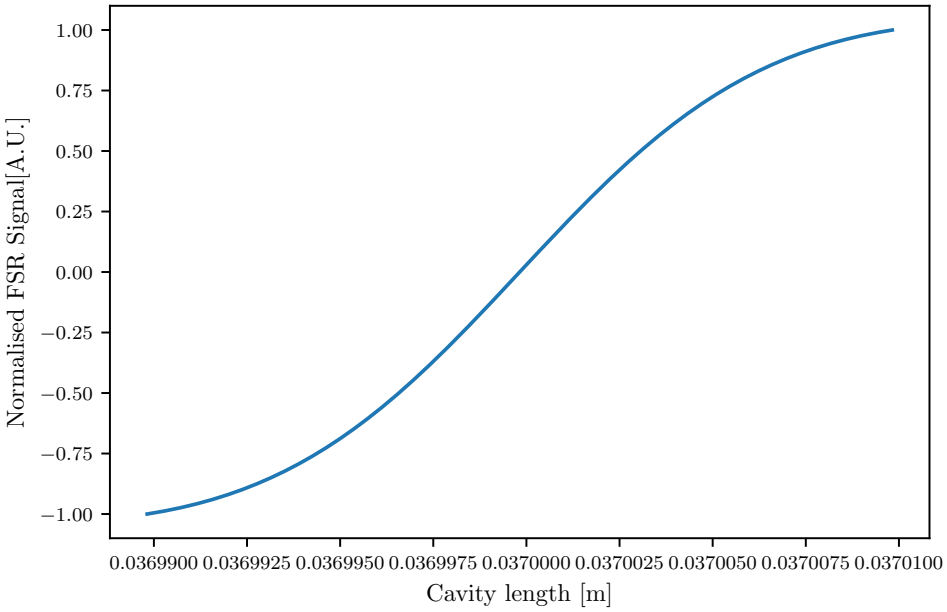

Figure B.3: Simulated free spectral range error signal.

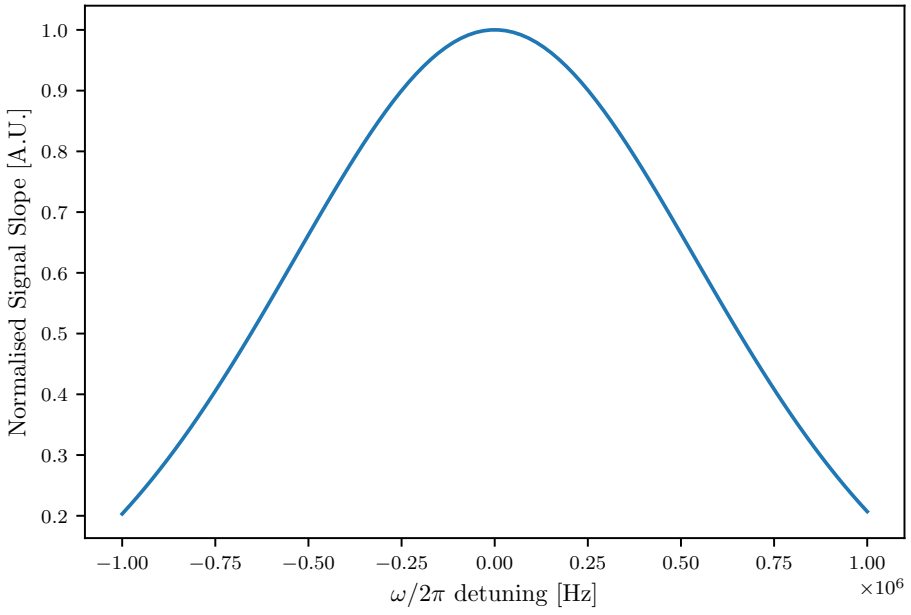

Figure B.4: Simulated free spectral range error signal slope with ω detuning.

Appendix C

Pyhton Code for Numerical Investigation of Free Spectral Range Lock Error Signal

```
#Simultaneous laser and cavity length stabilisation error
                                    signal investigation
#Deon Janse van Rensburg
#September 2020
import numpy as np
import matplotlib.pyplot as plt
from matplotlib import rc
from scipy import special as sp

rc('font',**{'family':'serif','serif':['Computer Modern']})
rc('text', usetex=True)
# fontsize of the axes title
plt.rc('xtick', labelsize=8)
plt.rc('ytick', labelsize=8)
plt.rc('legend', fontsize=12)
plt.rc('figure', titlesize=12)

r = 0.999 #Mirror Reflectance

#define reflection transfer function
def R(w,L):
return r*(np.exp(2*np.pi*1j*w/(cc/(2*L)))-1)/(1-r*r*np.exp(2*np
                                    .pi*1j*w/(cc/(2*L))))
```

```
#Carrier lock error signal
def pdh(a,b,c,alpha,beta,gamma,w,L):
return sp.jv(0,a)*sp.jv(1,a)*(sp.jv(0,b)**2*(R(w+alpha,L)*R(-w,
                                L)-R(-(w-alpha),L)*R(w,L))+sp.
                                jv(0,c)**2*sp.jv(1,b)**2*(
R(w+alpha+beta,L)*R(-(w+beta),L)-R(-(w-alpha+beta),L)*R(w+beta,
                                L)+R(w+alpha-beta,L)*R(-(w-beta
                                ),L)-R(-(w-alpha-beta),L)*R(w-
                                beta,L))
+sp.jv(1,c)**2*sp.jv(1,b)**2*(
R(w+alpha+beta+gamma,L)*R(-(w+beta+gamma),L)-R(-(w-alpha+beta+
                                gamma),L)*R(w+beta+gamma,L)+R(w
                                +alpha-beta+gamma,L)*R(-(w-beta
                                +gamma),L)-R(-(w-alpha-beta+
                                gamma),L)*R(w-beta+gamma,L)
+ R(w+alpha+beta-gamma,L)*R(-(w+beta-gamma),L)-R(-(w-alpha+beta
                                -gamma),L)*R(w+beta-gamma,L)+R(
                                w+alpha-beta-gamma,L)*R(-(w-
                                beta-gamma),L)-R(-(w-alpha-beta
                                -gamma),L)*R(w-beta-gamma,L))
                                                        )

#Free spectral range lock error signal
def fsr(a,b,c,alpha,beta,gamma,w,L):
return sp.jv(1,b)**2*sp.jv(0,c)*sp.jv(1,c)*(sp.jv(0,a)**2*(R(w+
                                beta+gamma,L)*R(-(w+beta),L)-R(
                                w-beta+gamma,L)*R(-(w-beta),L)
+ R(-(w-beta-gamma),L)*R((w-beta),L)-R(-(w+beta-gamma),L)*R((w+
                                beta),L))
+sp.jv(1,a)**2*(R(w+beta+gamma+alpha,L)*R(-(w+beta+alpha),L)-R(
                                w-beta+gamma+alpha,L)*R(-(w-
                                beta+alpha),L)
+ R(-(w+beta-gamma+alpha),L)*R((w+beta+alpha),L)-R(-(w-beta-
                                gamma+alpha),L)*R((w-beta+alpha
                                ),L)
+ R(w+beta+gamma-alpha,L)*R(-(w+beta-alpha),L)-R(w-beta+gamma-
                                alpha,L)*R(-(w-beta-alpha),L)
+ R(-(w+beta-gamma-alpha),L)*R((w+beta-alpha),L)-R(-(w-beta-
                                gamma-alpha),L)*R((w-beta-alpha
                                ),L)))
```

```
wl = 935*10**(-9) # wavelength of light (m)
cc = 299792458 # speed of light (m/s)
q = np.round(2*37*10**-3/wl)
cL= q*wl/2 # cavity length (m)
alpha = 12.5*10**6 #PDH modulation frequency(Hz)/ 2pi
beta = cc/(2*cL) #FSR modulation frequency(Hz)/ 2pi
gamma = 4*10**6 #FSR frequency modulation frequency(Hz)/ 2pi
a = 1.08 # PDH modulation depth
b = 1.84 # 4 GHz modulation depth
c = 1.08 # 4 MHz modulation depth

# Carrier Lock Error Signal, Scanning Laser
w=np.linspace(cc/wl-25*10**6,cc/wl+25*10**6,100000)#Laser
                                    frequency
plt.plot(w,np.imag(pdh(a,0,c,alpha,beta,gamma,w,cL))/np.max(np.
                                    imag(pdh(a,0,c,alpha,beta,gamma
                                    ,w,cL))),label="$b = 0$")
plt.plot(w,np.imag(pdh(a,1,c,alpha,beta,gamma,w,cL))/np.max(np.
                                    imag(pdh(a,0,c,alpha,beta,gamma
                                    ,w,cL))),label="$b = 1$")
plt.plot(w,np.imag(pdh(a,2,c,alpha,beta,gamma,w,cL))/np.max(np.
                                    imag(pdh(a,0,c,alpha,beta,gamma
                                    ,w,cL))),label="$b = 2$")
plt.plot(w,np.imag(pdh(a,3,0,alpha,beta,gamma,w,cL))/np.max(np.
                                    imag(pdh(a,0,c,alpha,beta,gamma
                                    ,w,cL))),label="$b = 3$")
plt.legend()
plt.ylabel("Signal Magnitude [A.U.]")
plt.xlabel("Laser Frequency [Hz]")
plt.savefig("PDHError.pdf", dpi=1200)
plt.clf()

#PDH Slope with detuned beta
w=np.linspace(cc/wl-1*10**6,cc/wl+1*10**6,100000)#Laser
                                    frequency
delta = np.linspace(-1*10**6,1*10**6,100)#Beta detuning
j = 0
slope = np.zeros(100)
for i in delta:
slope[j] = (np.imag(pdh(a,b,c,alpha,beta+i,gamma,w,cL))[50100]-
                                    np.imag(pdh(a,b,c,alpha,beta+i,
                                    gamma,w,cL))[49900])/(w[50100]-
```

```
                                    w[49900])
j+=1
plt.plot(delta,slope/np.max(slope))
plt.ylabel("Normalised Signal Slope [A.U.]")
plt.xlabel("$\\beta/2\\pi$ detuning [Hz]")
plt.savefig("PDHslope.pdf", dpi=1200)
plt.clf()

# FSR Lock Error Signal, Scanning Cavity Length
L = np.linspace(cL-10*10**-6, cL+10*10**-6, 100000)
plt.plot(L,np.imag(fsr(a,b,c,alpha,beta,gamma,q*cc/(2*L),L))/np
                                    .max(np.imag(fsr(a,b,c,alpha,
                                    beta,gamma,q*cc/(2*L),L))))
plt.ylabel("Normalised FSR Signal[A.U.]")
plt.xlabel("Cavity length [m]")
plt.savefig("FSRsignal.pdf", dpi=1200)
plt.clf()

#FSR Slope as function of carrier detuning
L=np.linspace(cL-1*10**-6,cL+1*10**-6,100000)#Laser frequency
delta = np.linspace(-1*10**6,1*10**6,100)#Beta detuning
j = 0
slope = np.zeros(100)
for i in delta:
slope[j] = (np.imag(fsr(a,b,c,alpha,beta,gamma,q*cc/(2*L)+i,L))
                                    [50100]-np.imag(fsr(a,b,c,alpha
                                    ,beta,gamma,q*cc/(2*L)+i,L))[
                                    49900])/(L[50100]-L[49900])
j+=1
plt.plot(delta,slope/np.max(slope))
plt.ylabel("Normalised Signal Slope [A.U.]")
plt.xlabel("$\\omega/2\\pi$ detuning [Hz]")
plt.savefig("FSRslope.pdf", dpi=1200)
plt.clf()
```

Bibliography

[1] Haroche, S. and Raimond, J.: *Exploring the Quantum*. Oxford University Press, 2006.

[2] Brewer, S., Chen, J.-S., Hankin, A., E.R., C., Chou, C., Wineland, D., Hume, D. and Leibrandt, D.: ^{27} Al $^{+}$ Quantum-Logic Clock with a Systematic Uncertainty below 10^{-18}. *Physical Review Letters*, vol. 123, 2019.

[3] Kielpinski, D., Monroe, C. and Wineland, D.: Architecture for a largescale iontrap quantum computer. *Nature*, vol. 417, 2002.

[4] Monroe, C., Meekhof, D.M., King, B., Itano, W.M. and Wineland, D.: Demonstration of a Fundamental Quantum Logic Gate. *Physical Review Letters*, vol. 75, no. 25, pp. 4714–4717, 1995.

[5] Foot, C.: *Atomic Physics*. Oxford University Press, 2014.

[6] Abbott, B. *et al.*: Observation of Gravitational Waves from a Binary Black Hole Merger. *Physical Review Letters*, vol. 116, 2016.

[7] Araya, A. *et al.*: Absolute-length determination of a long-baseline Fabry-Perot cavity by means of resonating modulation sidebands. *Applied Optics*, vol. 38, 1999.

[8] Ahmadi, A. *et al.*: Characterization of the 1S-2S transition in antihydrogen. *Nature*, vol. 557, 2018.

[9] CIAAW: Isotopic composition of the elements. url = http://www.ciaaw.org/isotopic-abundances.htm, 2017. Accessed: 2019-07-18.

[10] Kleinert, M., Gold Dahl, M. and Bergeson, S.: Measurement of the Yb I $^{1}S_{0}$-$^{1}P_{1}$ transition frequency at 399 nm using an optical frequency comb. *Physical Review A*, vol. 94, 2016.

[11] Berends, R., Pinnington, E., Guo, B. and Ji, Q.: Beam-laser lifetime measurements for four resonance levels of yb ii. vol. 26, 1993.

[12] Pinnington, E., Rieger, G. and Kernahan, J.: Beam-laser measurements of the lifetimes of the 6p levels in yb ii. vol. 56, no. 3, 1997.

[13] Tran, M.A., Huang, D. and Bowers, J.E.: Tutorial on narrow linewidth tunable semiconductor lasers using si/iii-v heterogeneous integration. *APL Photonics*, vol. 4, no. 11, 2019.

[14] Mooradian, A.: *Spectral Characteristics of Semiconductor Diode Lasers*. 1984.

[15] Stéphan, G.M., Tam, T.T., Blin, S., Besnard, P. and Têtu, M.: Laser line shape and spectral density of frequency noise. *Physical Review A*, 2005.

[16] Di Domenico, G., Schilt, S. and Thomann, P.: Simple approach to the relation between laser frequency noise and laser line shape. *Applied Optics*, vol. 49, 2010.

[17] Bucalovic, N., Dolgovskiy, V., Schori, C., Thomann, P., Di Domenico, G. and Schilt, S.: Experimental validation of a simple approximation to determine the linewidth of a laser from its frequency noise spectrum. *Applied Optics*, vol. 51, no. 20, 2012.

[18] Hinkley, E.D. and Freed, C.: Direct observation of the lorentzian line shape as limited by quantum phase noise in a laser above threshold. *Physical Review Letters*, vol. 23, no. 6, 1969.

[19] Okoshi, T., Kikuchi, K. and Nakayama, A.: Novel method for high resolution measurement of laser output spectrum. *Electronics Letters*, vol. 16, no. 16, 1980.

[20] Richter, L.E. and Mandelberg, H.I.: Linewidth determination from self-heterodyne measurements with subcoherence delay times. *Quantum Electronics Letters*, vol. 22, no. 11, 1986.

[21] Ludvigsen, H., Tossavainen, M. and Kaivola, M.: Laser linewidth measurements using self-homodyne detection with short delay. *Optics Communications*, 1998.

[22] Kikuchi, K. and Okoshi, T.: Dependence of semiconductor laser linewidth on measurement time: Evidence of predominance of of 1/f noise. *Electronics Letters*, vol. 21, no. 22, 1985.

[23] Huang, S., Zhu, T., Liu, M. and Huang, W.: Precise measurement of ultra-narrow laser linewidths using the strong coherent envelope. *Scientific Reports*, 2017.

[24] Fox, R.W., Oates, C.W. and Hollberg, L.W.: Stabilizing diode lasers to high-finesse cavities. In: van Zee, R.D. and Looney, J.P. (eds.), *Cavity-Enhanced Spectroscopies*, vol. 40 of *Experimental Methods in the Physical Sciences*, chap. 1, pp. 2–5. Elsevier, 2003.

[25] Visioli, A.: *Practical PID Control*. Springer, 2006.

[26] des Poids et Mesures, B.I.: *The International System of Units (SI)*. Ninth edn. 2019.

[27] *Ultra-Fast 100 GHz Photodetector*. Finisar, 2014. Rev. A1.

[28] Hirata, S., Akatsuka, T., Ohtake, Y. and Morinaga, A.: Sub-hertz-linewidth diode laser stabilized to an ultralow-drift high-finesse optical cavity. *Applied Physics Express*, 2014.

[29] Hodgson, N. and Weber, H.: *Optical Resonators*. Springer, 1997.

[30] Birch, K. and Downs, M.: An updated edlén equation for the refractive index of air. *Metrologia*, vol. 30, 1993.

[31] *ULE® Corning Code 7972 Ultra Low Expansion Glass*. Corning, 2008.

[32] Paquin, R.A.: *Materials for Optical Systems*. 1997.

[33] Drever, R., Hall, J.L., Kowalski, F.V., Hough, J., Ford, G.M., Munley, A.J. and Ward, H.: Laser phase and frequency stabilization using an optical resonator. *Applied Physics B*, vol. 31, 1983.

[34] Black, E.: An introduction to pound-drever-hall laser frequancy stabilisation. *American Journal of Physics*, vol. 69, 2001.

[35] Belfi, J., Beverini, N., Cuccato, D., Di Virgilio, A., Maccioni, N., Ortolan, A. and Santagata, R.: Interferometric length metrology for the dimensional control of ultra-stable ring laser gyroscopes. *Classical and Quantum Gravity*, vol. 31, no. 5, 2014.

[36] Sepiol, M.A.: *Frequency stabilization of a 729 nm diode laser to an external high finesse reference cavity*. Master's thesis, Swiss Federal Institute of Technology in Zurich, 2012.

[37] Lindsay, B.G., Smith, K.A. and Dunning, F.B.: Control of longterm output frequency drift in commercial dye lasers. *Review of Scientific Instruments*, vol. 61, no. 1656, 1991.

[38] Zhao, W.Z., Simsarian, J.E., Orozco, L.A. and Sprouse, G.D.: A computer-based digital feedback control of frequency drift of multiple lasers. *Review of Scientific Instruments*, vol. 69, no. 3737, 1998.

[39] Defoe, R.G. and Brewer, R.G.: Laser-frequency division and stabilization. *Physical Review A*, vol. 30, no. 5, 1984.

[40] Hagel, G., Houssin, M., Knoop, M., Champenois, C., Vedel, M. and Vedel, F.: Long-term stabilization of the length of an optical reference cavity. *Review of Scientific Instruments*, vol. 76, 2005.

[41] Smith, S. and D.G., C.: *Foundations of Ultraprecision Mechanism Design*, vol. 2. Gordon and Breach Science Publishers, 2005.

[42] Kogelnik, H. and Li, T.: Laser beams and resonators. vol. 5, no. 10, 1966.

[43] Morville, J., Romanini, D. Chenevier, M. and A., K.: Effects of laser phase noise on the injection of a high-finesse cavity. *Applied Optics*, vol. 41, no. 33, 2002.

[44] Millo, J., Magalhães, D.V., Mandache, C., Le Coq, Y., English, E.M.L., Westergaard, P.G., Lodewyck, J., Bize, S., Lemonde, P. and Santarelli, G.: Ultrastable lasers based on vibration insensitive cavities. *Physical Review A*, vol. 79, 2009.

[45] Fleming, M. and Mooradian, A.: Spectral characteristics of external-cavity controlled semiconductor lasers. vol. 17, no. 1, 1981.

[46] Lang, R. and Kobayashi, K.: External optical feedback effects on semiconductor injection laser properties. vol. 16, no. 3, 1980.

[47] Tkach, R. and Chraplyvy, A.: Regimes of feedback effects in 1.5-μm distributed feedback lasers. vol. 4, no. 11, 1986.

[48] *Datasheet and Operating Guide WTC3243 and WTC3293 Ultrastable TEC controller and Evaluation Board.* Wavelength Electronics, 2019.

[49] *Opaque Fluoroplastics PTFE Sheet Datasheet.* RS Pro, 2020.

[50] Graves, R.S., Kollie, T.G., McElroy, D.L. and E., G.K.: The thermal conductivity of aisi 304l stainless steel. *International Journal of Thermophysics*, vol. 12, no. 2, 1991.

[51] *USB-6008 Specifications*. National Instruments, 2017.

[52] Steele, J., Thompson, D., Jacobs, S. and Bass, D.: Temperature and age effects on the temporal stability of invar. *Proc. SPIE*, vol. 1752, 1992.

[53] Berthold, J.W., Jacobs, S.F. and Norton, M.A.: Dimensional stability of fused silica, invar, and several ultra-low thermal expansion materials. *Metrologia*, 1976.